

**AN EFFICIENT METHOD FOR DETERMINING ENERGY HARVESTING  
CAPABILITIES OF MULTIPLE ANTENNAS IN THE SAME SPACE**

by

**Justin Panuski**

B.S. in Electrical Engineering, University of Pittsburgh, 2006

Submitted to the Graduate Faculty of  
School of Engineering in partial fulfillment  
of the requirements for the degree of  
Master of Science

University of Pittsburgh

2007

UNIVERSITY OF PITTSBURGH

SCHOOL OF ENGINEERING

This thesis was presented

by

Justin Panuski

It was defended on

July 18, 2007

and approved by

Ronald G. Hoelzeman, Associate Professor, Electrical and Computer Engineering

Bryan A. Norman, Associate Professor, Industrial Engineering

Thesis Co-Advisor: James T. Cain, Professor, Electrical and Computer Engineering

Thesis Co-Advisor: Marlin H. Mickle, Nickolas A. DeCecco Professor, Electrical and Computer  
Engineering

Copyright © by Justin Panuski

2007

**AN EFFICIENT METHOD FOR DETERMINING ENERGY HARVESTING  
CAPABILITIES OF MULTIPLE ANTENNAS IN THE SAME SPACE**

Justin Panuski, M.S.

University of Pittsburgh, 2007

Passive energy harvesting is important for many applications, one of which is Radio Frequency Identification (RFID). For RFID applications the size of the tag is important, and as the chips performing the logic are small, the size of the tag is determined by the antenna. This research examines the effects of placing multiple antennas powering multiple RFID chips in a small area. Four new designs are proposed and examined to determine antenna design performance when placed in close proximity. A new method of evaluation is proposed involving the connection of Gen 2 RFID chips as a way to eliminate wire connections needed for measurements.

## TABLE OF CONTENTS

<b>1.0</b>	<b>STATEMENT OF THE PROBLEM .....</b>	<b>1</b>
<b>2.0</b>	<b>ENERGY HARVESTING.....</b>	<b>2</b>
<b>2.1</b>	<b>DESIGN .....</b>	<b>2</b>
<b>2.2</b>	<b>MATCHING .....</b>	<b>5</b>
<b>2.3</b>	<b>EVALUATION METHODS.....</b>	<b>11</b>
<b>3.0</b>	<b>VIRTUAL POWER METER RESULTS .....</b>	<b>14</b>
<b>3.1</b>	<b>MATCHING .....</b>	<b>14</b>
<b>3.2</b>	<b>PROCEDURAL RESULTS.....</b>	<b>19</b>
<b>3.2.1</b>	<b>Individual Element Measurements .....</b>	<b>20</b>
<b>3.2.2</b>	<b>Distance Measurements.....</b>	<b>22</b>
<b>3.2.3</b>	<b>Polarization Tests.....</b>	<b>23</b>
<b>3.3</b>	<b>EVALUATION .....</b>	<b>26</b>
<b>4.0</b>	<b>RFID TAGS .....</b>	<b>36</b>
<b>4.1</b>	<b>SIMULATION .....</b>	<b>37</b>
<b>4.2</b>	<b>DIRECT CONNECTION .....</b>	<b>43</b>
<b>4.3</b>	<b>CAPACITIVE COUPLING .....</b>	<b>44</b>
<b>4.4</b>	<b>EVALUATION METHODS.....</b>	<b>49</b>
<b>5.0</b>	<b>RFID TAG RESULTS .....</b>	<b>53</b>

<b>5.1</b>	<b>SIMULATION .....</b>	<b>53</b>
<b>5.2</b>	<b>DIRECT CONNECTION .....</b>	<b>55</b>
<b>5.3</b>	<b>CAPACITIVE COUPLING .....</b>	<b>59</b>
<b>5.3.1</b>	<b>Read Rate.....</b>	<b>59</b>
<b>5.3.2</b>	<b>Maximum Distance .....</b>	<b>64</b>
<b>6.0</b>	<b>CONCLUSION.....</b>	<b>70</b>
	<b>APPENDIX A .....</b>	<b>75</b>
	<b>APPENDIX B .....</b>	<b>91</b>
	<b>BIBLIOGRAPHY .....</b>	<b>122</b>

## LIST OF TABLES

Table 2.1. Uncenter Matching .....	11
Table 3.1. Sarlacc Matching .....	15
Table 3.2. Oculus Matching.....	16
Table 3.3. Uroboros Matching – Element 1.....	17
Table 3.4. Uroboros Matching – Element 2.....	18
Table 3.5. Uroboros Matching – Element 3.....	18
Table 3.6. Uroboros Matching – Element 4.....	19
Table 3.7. Individual Element Voltages – Minhong.....	20
Table 3.8. Individual Element Voltages – Uncenter.....	21
Table 3.9. Individual Element Voltages – Sarlacc.....	21
Table 3.10. Individual Element Voltages – Oculus .....	21
Table 3.11. Individual Element Voltages – Uroboros .....	22
Table 3.12. Measure Distance.....	22
Table 3.13. Sarlacc Polarization Test 1 .....	25
Table 3.14. Sarlacc Polarization Test 2 .....	25
Table 3.15. Sarlacc Polarization Test 3 .....	26
Table 3.16. Element Voltages Linear Polarization Position 1 – Minhong .....	27

Table 3.17. Element Voltages Linear Polarization Position 2 – Minhong .....	27
Table 3.18. Element Voltages Linear Polarization Position 3 – Minhong .....	28
Table 3.19. Element Voltages Linear Polarization Position 4 – Minhong .....	28
Table 3.20. Element Voltages Circular Polarization Position 1 – Minhong.....	31
Table 3.21. Element Voltages Circular Polarization Position 2 – Minhong.....	32
Table 3.22. Element Voltages Circular Polarization Position 3 – Minhong.....	32
Table 3.23. Element Voltages Circular Polarization Position 4 – Minhong.....	32
Table 3.24. VPM Distances – Linear Polarization .....	34
Table 3.25. VPM Distances – Circular Polarization.....	34
Table 4.1. Simulated Minhong Impedance .....	40
Table 5.1. Uncenter Simulation Results .....	53
Table 5.2. Sarlacc Simulation Results .....	54
Table 5.3. Oculus Simulation Results.....	54
Table 5.4. External Circular Polarization Position 1 – Sarlacc.....	56
Table 5.5. External Circular Polarization Position 2 – Sarlacc.....	56
Table 5.6. External Circular Polarization Position 3 – Sarlacc.....	56
Table 5.7. External Circular Polarization Position 4 – Sarlacc.....	57
Table 5.8. External Circular Polarization Position 1 – Minhong.....	57
Table 5.9. External Circular Polarization Position 2 – Minhong.....	58
Table 5.10. External Circular Polarization Position 3 – Minhong.....	58
Table 5.11. External Circular Polarization Position 4 – Minhong.....	58
Table 5.12. Read Rate Linear Polarization Position 1 – Sarlacc .....	60
Table 5.13. Read Rate Linear Polarization Position 2 – Sarlacc .....	60



Table 5.14. Read Rate Linear Polarization Position 3 – Sarlacc .....	61
Table 5.15. Read Rate Linear Polarization Position 4 – Sarlacc .....	61
Table 5.16. Read Rate Linear Polarization – TI Tag .....	61
Table 5.17. Read Rate Circular Polarization Position 1 – Sarlacc.....	62
Table 5.18. Read Rate Circular Polarization Position 2 – Sarlacc.....	62
Table 5.19. Read Rate Circular Polarization Position 3 – Sarlacc.....	63
Table 5.20. Read Rate Circular Polarization Position 4 – Sarlacc.....	63
Table 5.21. Read Rate Circular Polarization – TI Tag .....	63
Table 5.22. Read Range Linear Polarization Position 1 – Sarlacc .....	65
Table 5.23. Read Range Linear Polarization Position 2 – Sarlacc .....	65
Table 5.24. Read Range Linear Polarization Position 3 – Sarlacc .....	65
Table 5.25. Read Range Linear Polarization Position 4 – Sarlacc .....	66
Table 5.26. Read Range Linear Polarization – TI Tag .....	66
Table 5.27. Read Range Circular Polarization Position 1 – Sarlacc.....	67
Table 5.28. Read Range Circular Polarization Position 2 – Sarlacc.....	67
Table 5.29. Read Range Circular Polarization Position 3 – Sarlacc.....	68
Table 5.30. Read Range Circular Polarization Position 4 – Sarlacc.....	68
Table 5.31. Read Range Circular Polarization – TI Tag.....	68
Table 6.1. Summary of Results.....	71
Table 6.2. Overall Design Rank.....	73
Table A6.3. Element Voltages Linear Polarization Position 1 – Minhong .....	75
Table A6.4. Element Voltages Linear Polarization Position 2 – Minhong .....	76
Table A6.5. Element Voltages Linear Polarization Position 3 – Minhong .....	76

Table A6.6. Element Voltages Linear Polarization Position 4 – Minhong .....	76
Table A6.7. Element Voltages Linear Polarization Position 1 – Uncenter .....	77
Table A6.8. Element Voltages Linear Polarization Position 2 – Uncenter .....	77
Table A6.9. Element Voltages Linear Polarization Position 3 – Uncenter .....	77
Table A6.10. Element Voltages Linear Polarization Position 4 – Uncenter .....	78
Table A6.11. Element Voltages Linear Polarization Position 1 – Sarlacc .....	78
Table A6.12. Element Voltages Linear Polarization Position 2 – Sarlacc .....	79
Table A6.13. Element Voltages Linear Polarization Position 3 – Sarlacc .....	79
Table A6.14. Element Voltages Linear Polarization Position 4 – Sarlacc .....	79
Table A6.15. Element Voltages Linear Polarization Position 1 – Oculus.....	80
Table A6.16. Element Voltages Linear Polarization Position 2 – Oculus.....	80
Table A6.17. Element Voltages Linear Polarization Position 3 – Oculus.....	80
Table A6.18. Element Voltages Linear Polarization Position 4 – Oculus.....	81
Table A6.19. Element Voltages Linear Polarization Position 1 – Uroboros.....	81
Table A6.20. Element Voltages Linear Polarization Position 2 – Uroboros.....	82
Table A6.21. Element Voltages Linear Polarization Position 3 – Uroboros.....	82
Table A6.22. Element Voltages Linear Polarization Position 4 – Uroboros.....	82
Table A6.23. Element Voltages Circular Polarization Position 1 – Minhong.....	83
Table A6.24. Element Voltages Circular Polarization Position 2 – Minhong.....	83
Table A6.25. Element Voltages Circular Polarization Position 3 – Minhong.....	84
Table A6.26. Element Voltages Circular Polarization Position 4 – Minhong.....	84
Table A6.27. Element Voltages Circular Polarization Position 1 – Uncenter.....	85
Table A6.28. Element Voltages Circular Polarization Position 2 – Uncenter.....	85

Table A6.29. Element Voltages Circular Polarization Position 3 – Uncenter.....	85
Table A6.30. Element Voltages Circular Polarization Position 4 – Uncenter.....	86
Table A6.31. Element Voltages Circular Polarization Position 1 – Sarlacc.....	86
Table A6.32. Element Voltages Circular Polarization Position 2 – Sarlacc.....	87
Table A6.33. Element Voltages Circular Polarization Position 3 – Sarlacc.....	87
Table A6.34. Element Voltages Circular Polarization Position 4 – Sarlacc.....	87
Table A6.35. Element Voltages Circular Polarization Position 1 – Oculus .....	88
Table A6.36. Element Voltages Circular Polarization Position 2 – Oculus .....	88
Table A6.37. Element Voltages Circular Polarization Position 3 – Oculus .....	88
Table A6.38. Element Voltages Circular Polarization Position 4 – Oculus .....	89
Table A6.39. Element Voltages Circular Polarization Position 1 – Uroboros .....	89
Table A6.40. Element Voltages Circular Polarization Position 2 – Uroboros .....	90
Table A6.41. Element Voltages Circular Polarization Position 3 – Uroboros .....	90
Table A6.42. Element Voltages Circular Polarization Position 4 – Uroboros .....	90
Table B6.43. Read Rate Linear Polarization Position 1 – Uncenter.....	92
Table B6.44. Read Rate Linear Polarization Position 2 – Uncenter.....	92
Table B6.45. Read Rate Linear Polarization Position 3 – Uncenter.....	93
Table B6.46. Read Rate Linear Polarization Position 4 – Uncenter.....	93
Table B6.47. Read Rate Linear Polarization Position 1 – Sarlacc.....	94
Table B6.48. Read Rate Linear Polarization Position 2 – Sarlacc.....	94
Table B6.49. Read Rate Linear Polarization Position 3 – Sarlacc.....	95
Table B6.50. Read Rate Linear Polarization Position 4 – Sarlacc.....	95
Table B6.51. Read Rate Linear Polarization Position 1 – Oculus .....	96

Table B6.52. Read Rate Linear Polarization Position 2 – Oculus .....	96
Table B6.53. Read Rate Linear Polarization Position 3 – Oculus .....	97
Table B6.54. Read Rate Linear Polarization Position 4 – Oculus .....	97
Table B6.55. Read Rate Linear Polarization – TI Tag .....	98
Table B6.56. Read Rate Circular Polarization Position 1 – Uncenter .....	98
Table B6.57. Read Rate Circular Polarization Position 2 – Uncenter .....	99
Table B6.58. Read Rate Circular Polarization Position 3 – Uncenter .....	99
Table B6.59. Read Rate Circular Polarization Position 4 – Uncenter .....	100
Table B6.60. Read Rate Circular Polarization Position 1 – Sarlacc .....	100
Table B6.61. Read Rate Circular Polarization Position 2 – Sarlacc .....	101
Table B6.62. Read Rate Circular Polarization Position 3 – Sarlacc .....	101
Table B6.63. Read Rate Circular Polarization Position 4 – Sarlacc .....	102
Table B6.64. Read Rate Circular Polarization Position 1 – Oculus .....	102
Table B6.65. Read Rate Circular Polarization Position 2 – Oculus .....	103
Table B6.66. Read Rate Circular Polarization Position 3 – Oculus .....	103
Table B6.67. Read Rate Circular Polarization Position 4 – Oculus .....	104
Table B6.68. Read Rate Circular Polarization– TI Tag.....	104
Table B6.69. Read Range Linear Polarization Position 1 – Minhong.....	105
Table B6.70. Read Range Linear Polarization Position 2 – Minhong.....	105
Table B6.71. Read Range Linear Polarization Position 3 – Minhong.....	106
Table B6.72. Read Range Linear Polarization Position 4 – Minhong.....	106
Table B6.73. Read Range Linear Polarization Position 1 – Uncenter.....	107
Table B6.74. Read Range Linear Polarization Position 2 – Uncenter.....	107

Table B6.75. Read Range Linear Polarization Position 3 – Uncenter .....	108
Table B6.76. Read Range Linear Polarization Position 4 – Uncenter .....	108
Table B6.77. Read Range Linear Polarization Position 1 – Sarlacc .....	109
Table B6.78. Read Range Linear Polarization Position 2 – Sarlacc .....	109
Table B6.79. Read Range Linear Polarization Position 3 – Sarlacc .....	110
Table B6.80. Read Range Linear Polarization Position 4 – Sarlacc .....	110
Table B6.81. Read Range Linear Polarization Position 1 – Oculus .....	111
Table B6.82. Read Range Linear Polarization Position 2 – Oculus .....	111
Table B6.83. Read Range Linear Polarization Position 3 – Oculus .....	112
Table B6.84. Read Range Linear Polarization Position 4 – Oculus .....	112
Table B6.85. Read Range Linear Polarization– TI Tag.....	113
Table B6.86. Read Range Circular Polarization Position 1 – Minhong .....	113
Table B6.87. Read Range Circular Polarization Position 2 – Minhong .....	114
Table B6.88. Read Range Circular Polarization Position 3 – Minhong .....	114
Table B6.89. Read Range Circular Polarization Position 4 – Minhong .....	115
Table B6.90. Read Range Circular Polarization Position 1 – Uncenter .....	115
Table B6.91. Read Range Circular Polarization Position 2 – Uncenter .....	116
Table B6.92. Read Range Circular Polarization Position 3 – Uncenter .....	116
Table B6.93. Read Range Circular Polarization Position 4 – Uncenter .....	117
Table B6.94. Read Range Circular Polarization Position 1 – Sarlacc .....	117
Table B6.95. Read Range Circular Polarization Position 2 – Sarlacc .....	118
Table B6.96. Read Range Circular Polarization Position 3 – Sarlacc .....	118
Table B6.97. Read Range Circular Polarization Position 4 – Sarlacc .....	119

Table B6.98. Read Range Circular Polarization Position 1 – Oculus .....	119
Table B6.99. Read Range Circular Polarization Position 2 – Oculus .....	120
Table B6.100. Read Range Circular Polarization Position 3 – Oculus .....	120
Table B6.101. Read Range Circular Polarization Position 4 – Oculus .....	121
Table B6.102. Read Range Circular Polarization– TI Tag .....	121

## LIST OF FIGURES

Figure 2.1. Minhong PCB Express Layout.....	2
Figure 2.2. Minhong Antenna.....	2
Figure 2.3. Uncenter PCB Express Layout.....	3
Figure 2.4. Uncenter Design .....	3
Figure 2.5. Sarlacc PCB Express Layout.....	4
Figure 2.6. Sarlacc Design .....	4
Figure 2.7. Oculus PCB Express Layout .....	4
Figure 2.8. Oculus Design .....	4
Figure 2.9. Uroboros PCB Express Layout .....	5
Figure 2.10. Uroboros Design.....	5
Figure 2.11. Test Setup .....	6
Figure 2.12. Vector Network Anaylzer.....	7
Figure 2.13. Smith Chart with Uncenter Matching.....	8
Figure 2.14. Measurement Devices .....	10
Figure 2.15. VPM Measurement Setup.....	12
Figure 3.1. Sarlacc Polarization Test 1 .....	24
Figure 3.2. Wire Connection – Bottom Left.....	29

Figure 3.3. Wire Connection – Bottom Right.....	30
Figure 3.4. Wire Connection – Top Right .....	30
Figure 3.5. Wire Connection – Top Left.....	31
Figure 4.1. TI Loop.....	36
Figure 4.2. TI Strap.....	37
Figure 4.3. Minhong Board Cut with Dremel.....	38
Figure 4.4. Ansoft HFSS Simulation Environment .....	39
Figure 4.5. Minhong Design in Ansoft HFSS.....	40
Figure 4.6. Uncenter Design in Ansoft HFSS.....	41
Figure 4.7. Sarlacc Design in Ansoft HFSS .....	42
Figure 4.8. Oculus Design in Ansoft HFSS.....	42
Figure 4.9. Uroboros Design in Ansoft HFSS .....	43
Figure 4.10. Sarlacc Board in Anechoic Chamber .....	44
Figure 4.11. Diagram Showing Coupling.....	45
Figure 4.12. Oculus Coupling Layout.....	46
Figure 4.13. Minhong Design with Coupling .....	47
Figure 4.14. Uncenter with Coupling .....	48
Figure 4.15. Sarlacc with Coupling .....	48
Figure 4.16. Oculus with Coupling.....	49
Figure 4.17. Max Read Range Setup .....	51
Figure 5.1. Circularly Polarized Sarlacc Test .....	55



## **1.0 STATEMENT OF THE PROBLEM**

Energy harvesting for electronic circuits often involves passive devices powered by Radio Frequency (RF) energy. Initial work in energy harvesting with multiple antennas [1, 2] has demonstrated that those antennas can be collocated without detrimental affects and combined to produce the sum of the individual energies (voltages).

The harvested energy may be used to power a sensor, RFID tag, etc. and the result communicated to a base station.

The problem to be addressed in this thesis is to; (1) Analyze a number of antenna topologies to discover factors that suggest a novel research direction, and to (2) analyze these topologies in a function form, i.e., an RFID tag using multiple antennas and silicon chips.

The original antenna design [1] will be augmented with four candidate designs where each design is chosen to exploit a particular aspect of a commercial application. Thus, each design will be tested for energy harvesting and as a multiple antenna, multiple chip RFID tag.

It is assumed, as indicated previously that based on prior research [1], the energies can be summed together by the previous methods. The research reported in this thesis is to determine the relative effects of one antenna on the other three in a four antenna configuration. In general, the objective is to determine the operating characteristics under different powering mechanisms for various orientations and topologies.

## 2.0 ENERGY HARVESTING

All of the antenna designs produced are extensions of an original design by Minhong Mi [1]. The desire to reduce the area taken up by the antenna drove the selection of new designs. Shown below is the original Minhong antenna combination with four individual antenna designs [1]. The research will maintain a four antenna combination with obvious four directional symmetry.

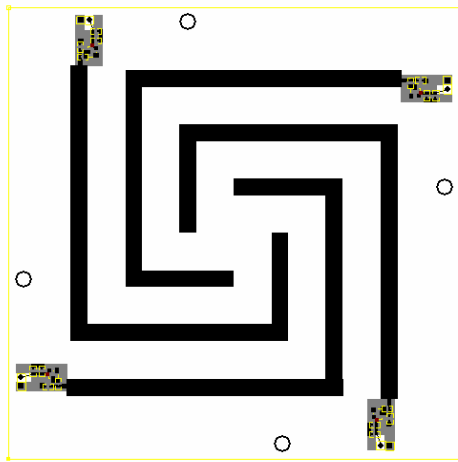


**Figure 2.1.** Minhong PCB Express Layout

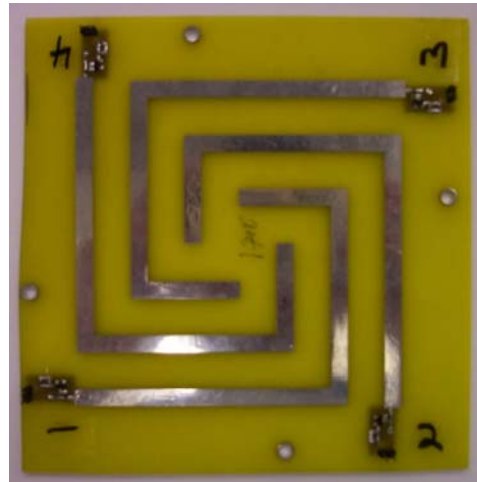


**Figure 2.2.** Minhong Antenna

## 2.1 DESIGN

The four new antenna designs are the result of evolutionary changes to the original design by Minhong Mi with the goal of making the antenna cover a smaller area and providing connections

(ports) on an outside or an inside basis. The antennas of Figure 2.1 and Figure 2.2 are four asymmetric dipoles matched for maximum energy. First, the antenna elements were moved together until they were almost touching leaving a square opening in the center without changing the length or shape of the original antennas. This choice changes one major factor – separation. The Uncenter board is shown below in Figure 2.3 and Figure 2.4.

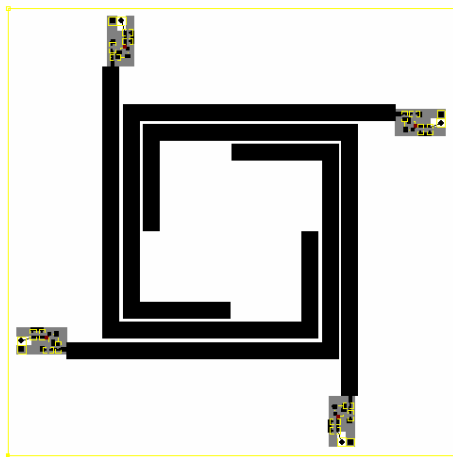


**Figure 2.3.** Uncenter PCB Express Layout

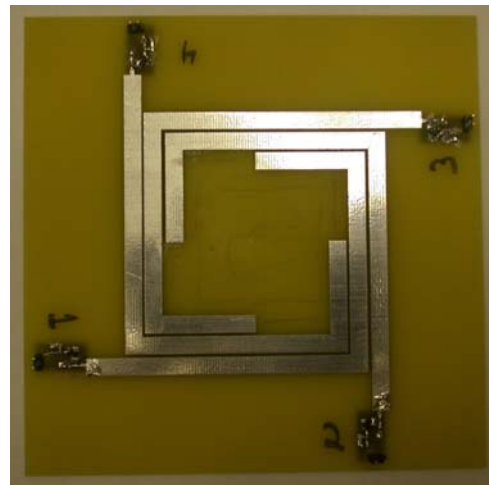


**Figure 2.4.** Uncenter Design

Next, in order to make the antenna any smaller, changes had to be made to the original antenna element structure. The first step was to fill in the open square; creating elements that spiraled out from the center, but were no longer a half wavelength long to maintain a square (patch type) appearance. This antenna is termed Sarlacc and is shown below in Figure 2.5 and Figure 2.6.

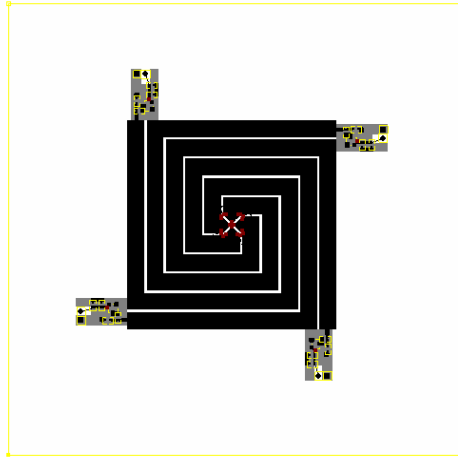


**Figure 2.5.** Sarlacc PCB Express Layout



**Figure 2.6.** Sarlacc Design

The next design was made with the idea of making it easier to connect the energy harvesting circuits to a single circuit/chip, either in series or parallel, by placing the connection points closer together. To do this, the harvesting circuits were placed at the center with the elements spiraling outward (instead of inward as done previously), thus creating the Oculus shown in Figure 2.7 and Figure 2.8.

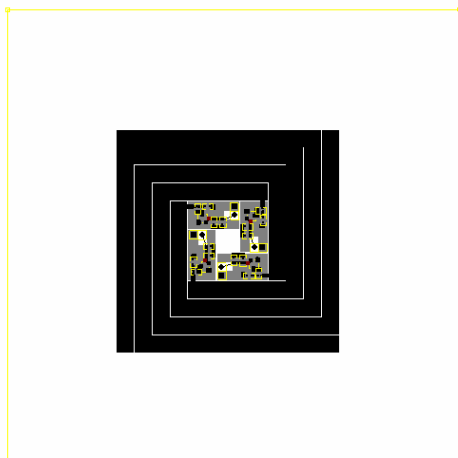


**Figure 2.7.** Oculus PCB Express Layout



**Figure 2.8.** Oculus Design

The fourth and final design was somewhat more whimsical. Here the elements were placed into one continuous spiral emanating from the center. This antenna, Uroboros, is pictured below in Figure 2.9 and Figure 2.10.

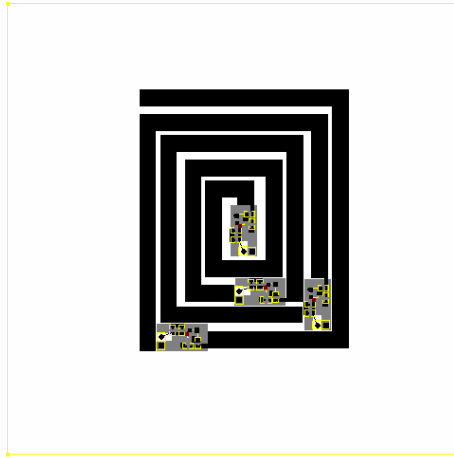


**Figure 2.9.** Uroboros PCB Express Layout

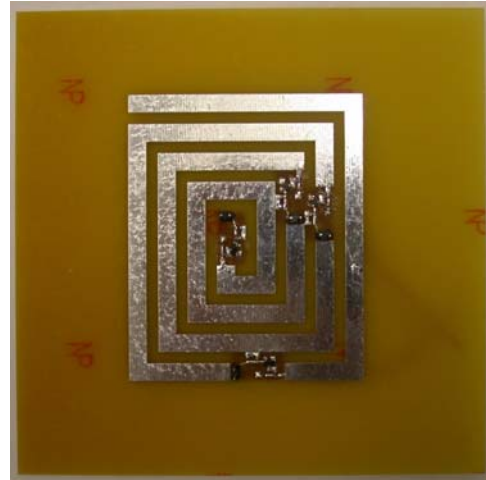


**Figure 2.10.** Uroboros Design

In all cases the lengths of the antennas were made as close to a half wavelength of a 915MHz wave as reasonably possible while still maintaining the desired square shape.

## 2.2 MATCHING

In order for maximum energy transfer to the harvesting circuit, each antenna was matched by hand using an iterative method developed by Minhong Mi and making use of the Virtual Power Meter (VPM) he designed [1]. In the case of the Uncenter, Sarlacc, and Oculus designs only one circuit was matched and then duplicated for all other elements, this is due to the symmetry of the elements. The point here is to determine the relative effects between the four elements when

they all have the same matching circuit. The symmetry implies that there is no “best” choice for which antenna element to match to as they are essentially identical. As the Uroboros design lacks any symmetry each of its elements was matched individually from the inside out.

This method uses two circuit boards, a measurement device / IR transmitter, and an IR receiver connected via a serial cable to a PC running a Matlab program, which displays the results. This extra effort of an IR link was done to minimize the cable load of a measurement device on the circuit and thus reduce any impact of performing the measurement on the actual value being measured. A picture of the VPM configuration is shown in Figure 2.11. On the left is the transmitting antenna, on the right is the design currently being tested, and in the back are the power supplies for the IR receiver board and the RF source.

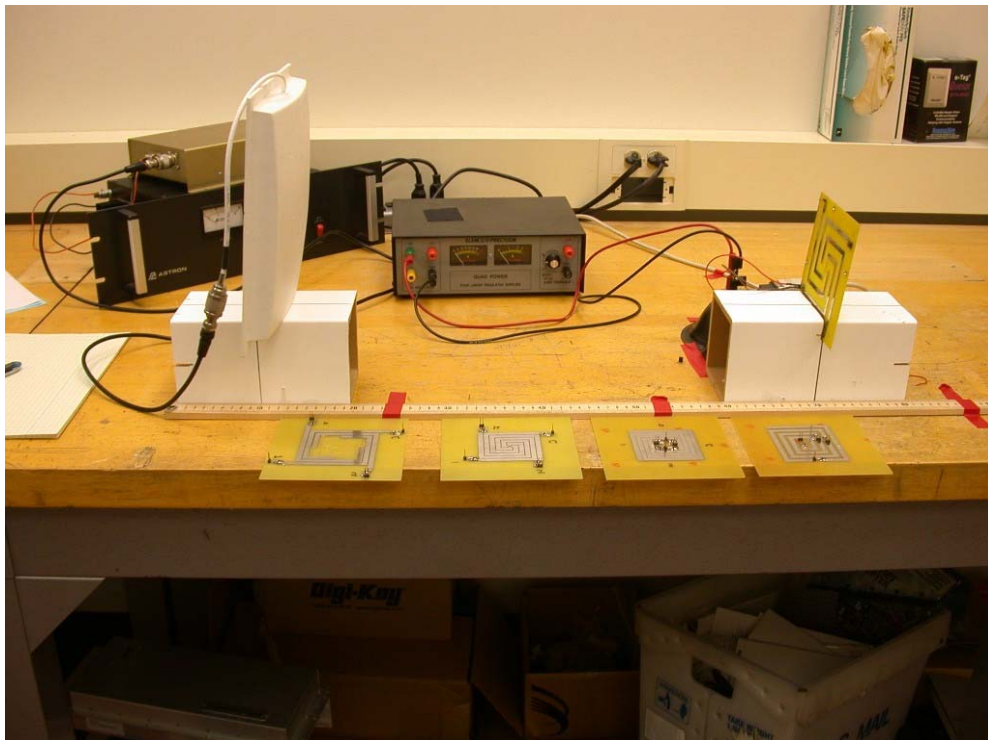


**Figure 2.11.** Test Setup

The matching was performed with the transmitter and element under test 25 inches apart. The transmitter consisted of a square patch, linearly polarized antenna connected to a 0.5 Watt, 915MHz, continuous wave source. Wires connecting the various pieces of equipment were taped down to prevent movement and ensure uniformity during testing. Also, marks were placed on the table top to designate the location of the transmitter and test antenna so that they could be properly aligned after having been moved to solder new components to the antenna element.

With the VPM setup, the process of matching could begin. First, a capacitor and inductor value were selected and soldered to the small board shown below so that their impedance could be measured on a Vector Network Analyzer and in turn plotted on a Smith Chart. The Vector Network Analyzer and attached measurement board are shown in Figure 2.12 below.



**Figure 2.12.** Vector Network Analyzer

An example Smith chart is shown in Figure 2.13 using impedance values from matching the Uncenter design with their corresponding voltages. It can be seen in the figure that the inductor choices determine the radius of a circle, and the capacitor values move along its

circumference. This chart can be used to pick values for testing because the impedance of the inductor and capacitor pair never change. If 18nH and 1pF is the current maximum, and it needed to be verified, the chart shows that 15nH and no capacitor is actually a better value to test than 15nH and 1pF because it is closer to the current maximum of 18nH and 1pF, which would not be obvious without plotting the values. It is also known that there is only one complex conjugate pair that will match the energy harvesting circuit to the antenna element and that once a maximum is verified further measurements involving more capacitor and inductor pairs is unnecessary.

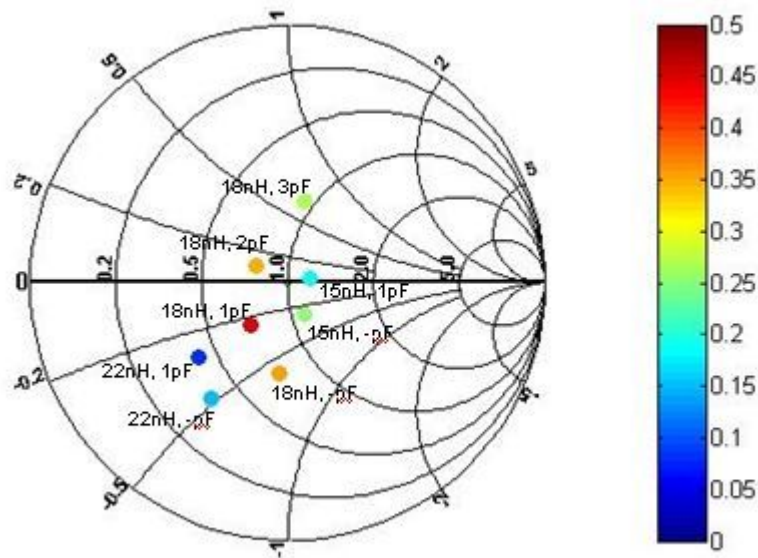


**Figure 2.13.** Smith Chart with Uncenter Matching

After this was done, the inductor and capacitor were transferred to the antenna element, which was then connected to the VPM, and a measurement of the voltage taken and recorded. The measurement was taken as an average over 10 stable samples after the initial transient from turning on the source. In this case the Smith Chart was a graphical tool to help visualize the



effect of changing the capacitor and/or inductor and the resulting change in measured voltage so that the matching could be achieved in fewer attempts as this can be a tedious process. This first round of matching was performed with integer values of capacitance. Once the best integer value was found a second round of matching was performed using capacitors with sub integer values.

Table 2.1 illustrates the series of measurements taken in the course of matching the Uncenter design. As the second set of measurements using the sub integer capacitors was often taken at a different time and all measurements were done outside of an anechoic chamber; therefore, the best performing integer case was measured again as a normalization to account for temperature and other fluctuations in the room and allow it to be used for comparison to the non integer measurements in determining the best matching. The gap in the table distinguishes these two different measurement sets. Figure 2.14 shows a close up of the measurement instrumentation with the Minhong design. There are two measurement boards in the picture. The board on the left against the white block measures the voltage harvest from the circuit and transmits it using an IR link to the second board which is connect by a serial cable to the computer running Matlab.

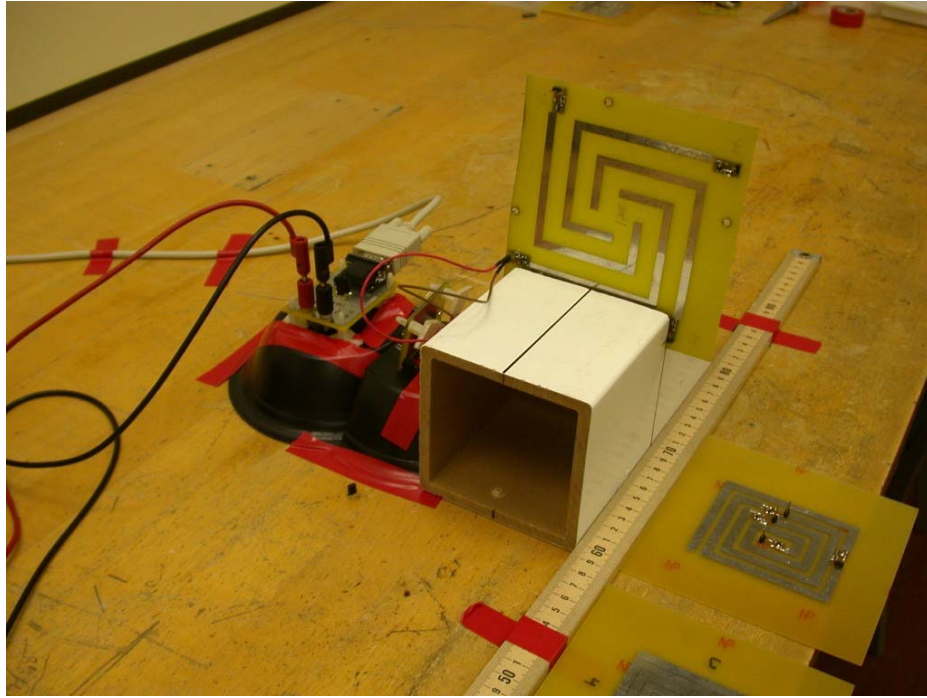


**Figure 2.14.** Measurement Devices

**Table 2.1.** Uncenter Matching

Inductor (nH)	Capacitor (pF)	Voltage (mV)
18	3	272.75
18	2	349.98
<b>18</b>	<b>1</b>	<b>446.27</b>
18	none	357.38
22	none	153.48
22	1	85.07
15	1	191.12
15	none	252.71
18	none	321.14
18	1	333.36
<b>18</b>	<b>1.5</b>	<b>401.30</b>
18	1.2	375.40
18	1.8	327.50

### 2.3 EVALUATION METHODS

Once all of the antennas were matched and setup properly, they were evaluated by two methods for comparison. First, each of the four elements of all five designs will be measured in all four possible orientations with each of two energy source antennas (linearly and circularly polarized), for a grand total of 160 measurements. The setup is similar to that used for the matching, a 0.5W

915MHz continuous wave source, but with a distance of 60cm. The distance changed because units were switched to metric for all measurements after the matching had been accomplished. Again voltage measurements would be taken using the VPM. Figure 2.15 shows the setup.

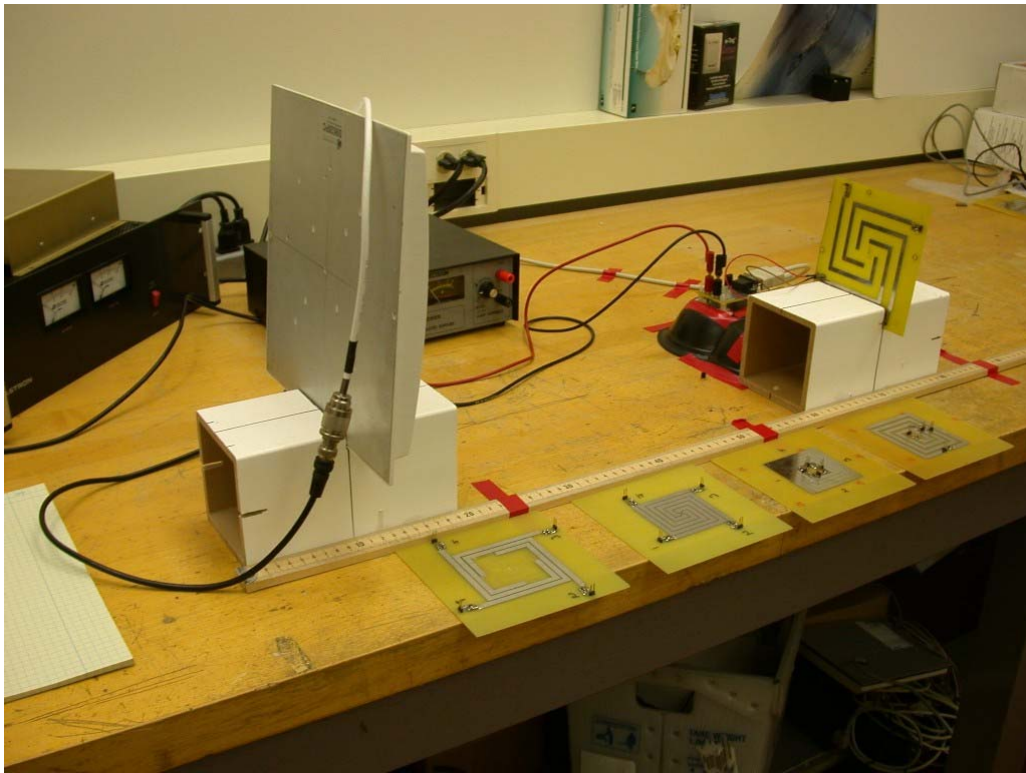


**Figure 2.15.** VPM Measurement Setup

The second test would be a distance measurement. These measurements were carried out by connecting the elements of each antenna design in series such that their voltages added together. The VPM measurement instrument saturates at 5v. Thus, to differentiate the candidates, the transmitter was moved farther and farther from each of the antennas until the VPM registered a value just under the 5v saturation. This gives a fundamental measurement of distance which is critical in most applications. In the case of the Uroboros board which is

asymmetrical, the elements were connected in series such that power was provided from the antenna at the center.

### **3.0 VIRTUAL POWER METER RESULTS**

#### **3.1 MATCHING**

Table 3.1 - Table 3.6 contain the measurements taken during the matching process for each of the new antenna designs. As described in Section 2.2 the Tables are broken into two parts: first, the integer matching portion and second, the non-integer matching. During the non-integer matching the best integer match is repeated to account for changes in the environment and allow comparisons

**Table 3.1.** Sarlacc Matching

Inductor (nH)	Capacitor (pF)	Voltage (mV)
22	3	628.60
22	2	791.37
22	1	919.92
22	none	1159.43
18	none	1037.72
18	1	939.07
24	1	1086.11
<b>24</b>	<b>none</b>	<b>1228.31</b>
27	none	1222.98
27	1	1019.61
24	none	1211.21
<b>24</b>	<b>0.1</b>	<b>1223.47</b>
24	0.3	1217.60
24	0.5	1153.75

**Table 3.2.** Oculus Matching

Inductor (nH)	Capacitor (pF)	Voltage (mV)
22	2	924.81
22	3	666.72
<b>22</b>	<b>1</b>	<b>1066.56</b>
22	none	960.00
24	1	917.70
24	none	972.71
24	2	933.12
27	2	813.36
27	1	1021.10
27	none	897.93
18	none	698.01
18	1	828.12
18	2	745.86
<b>22</b>	<b>1</b>	<b>877.78</b>
22	none	780.12
22	0.5	821.18
22	0.7	859.98
22	0.9	833.17
22	1.5	797.23
22	1.1	855.98



**Table 3.3.** Uroboros Matching – Element 1

Element #1		
Inductor (nH)	Capacitor (pF)	Voltage (mV)
18	2	416.46
18	3	346.96
18	1	531.75
18	none	589.98
22	none	734.67
22	1	641.31
24	none	830.47
24	1	631.53
<b>27</b>	<b>none</b>	<b>867.20</b>
27	1	527.44
30	1	378.82
30	none	779.15
<b>27</b>	<b>none</b>	<b>871.53</b>
27	0.1	829.49

**Table 3.4.** Uroboros Matching – Element 2

Element #2		
Inductor (nH)	Capacitor (pF)	Voltage (mV)
<b>27</b>	<b>none</b>	<b>1179.47</b>
27	0.1	1141.35
24	none	1036.23
30	none	

**Table 3.5.** Uroboros Matching – Element 3

Element #3		
Inductor (nH)	Capacitor (pF)	Voltage (mV)
27	none	998.13
27	0.1	1020.61
<b>27</b>	<b>0.3</b>	<b>1030.66</b>
27	0.7	990.20
27	0.5	1030.39
24	0.5	1010.84
24	0.3	1005.77
30	0.3	1028.92
30	0.5	986.89

**Table 3.6.** Uroboros Matching – Element 4

Element #4		
Inductor (nH)	Capacitor (pF)	Voltage (mV)
27	0.5	867.13
27	none	960.18
27	0.1	962.45
27	0.3	934.54
24	none	880.33
24	0.1	877.77
30	0.1	990.31
<b>30</b>	<b>none</b>	<b>1001.06</b>
33	none	912.43

### **3.2 PROCEDURAL RESULTS**

The results of this section were compiled while checking that the antenna elements were properly soldered and that all of the circuit components were functioning properly. As these tests were only done to verify that the designs were functioning they are repeated in a more formal manner in Section 3.3 and it is from these results that conclusions are drawn.

### 3.2.1 Individual Element Measurements

The tables below illustrate the resulting voltages measured with the VPM from each of the four elements of the designs. These measurements were taken under the same conditions as the matching; a 0.5W 915MHz continuous wave transmitter at a distance of 25 inches. After each measurement, the antenna design was rotated so that the measured element was always on the left. The Minhong and Sarlacc designs have only a 30mV difference between the highest and lowest value, while the Oculus and Uncenter have a 100mV difference, and the Uroboros has the most variance at 200mV. As the soldering was done by hand, the variation of each element's result is in a large part likely due to inconsistencies in soldering. Placement of the wires used for measurement may also have had a minor effect.

**Table 3.7.** Individual Element Voltages – Minhong

Element	Voltage (mV)
1	903.30
2	916.99
3	919.43
4	935.07

**Table 3.8.** Individual Element Voltages – Uncenter

Element	Voltage (mV)
1	335.32
2	319.68
3	256.62
4	365.62

**Table 3.9.** Individual Element Voltages – Sarlace

Element	Voltage (mV)
1	1191.69
2	1160.41
3	1181.92
4	1193.16

**Table 3.10.** Individual Element Voltages – Oculus

Element	Voltage (mV)
1	408.15
2	477.36
3	371.49
4	446.26

**Table 3.11.** Individual Element Voltages – Uroboros

Element	Voltage (mV)
1	821.67
2	705.34
3	849.53
4	906.24

### 3.2.2 Distance Measurements

These measurements were carried out by connecting the elements of each antenna design in series such that their voltages added together. As described in Section 2.3, the transmitter was moved farther and farther from each of the antennas until the VPM registered a value just under the 5v saturation.

**Table 3.12.** Measure Distance

Antenna Design	Distance (inches)
Minhong	38.6
Uncenter	36
Sarlacc	18.4
Oculus	13.2
Uroboros	32.8

In all cases the voltage increased at a given distance due to the series connections. However, there is one observation to be drawn from the table that is not consistent with what would be expected. One would expect that, as the elements are only connected in series now, the designs would have the same ranking as they did in the individual tests. Namely that Sarlacc which had the highest individual voltage would have the farthest distance before dropping below 5v. However, this is not the case. The Uncenter board, which performed the worst individually, had a distance measurement twice that of Sarlacc. It is conjectured that this is due to the constructive and destructive interference being different in each design. In the Sarlacc and Oculus designs, where the elements are very close together, there is more destructive interference. This seems plausible as both performed very poorly. For the Uncenter board, somehow the elements are spaced such that they work together and become greater than the sum of its individual elements.

The final answer to this question is a topic outside of this thesis, requiring a detailed analysis of the current and voltage patterns within the antenna elements then solving for them analytically or through simulations using tools such as those provided by Ansoft.

### **3.2.3 Polarization Tests**

Due to the anomaly pointed out in Section 0, doubt was cast as to the validity of the measurements based on the polarization of the energizing antenna. The antenna used for testing was not circularly polarized. This does not affect any of the previous results (such as matching), but might possibly explain why the distance values were unexpected. A series of tests was performed on the Sarlacc antenna using a circularly polarized antenna.

First, a test was run to verify the antenna was in fact circularly polarized. This was done by placing the Sarlacc 25 inches away, as done previously, with element number 1 on the left and measuring the voltage output from each element without rotating anything. Due to the symmetry of the antenna and the circular polarization of the transmitter, each element should report the same voltage. Figure 3.1 depicts the setup with the Sarlacc design. In the picture antenna element 3 is being measured.

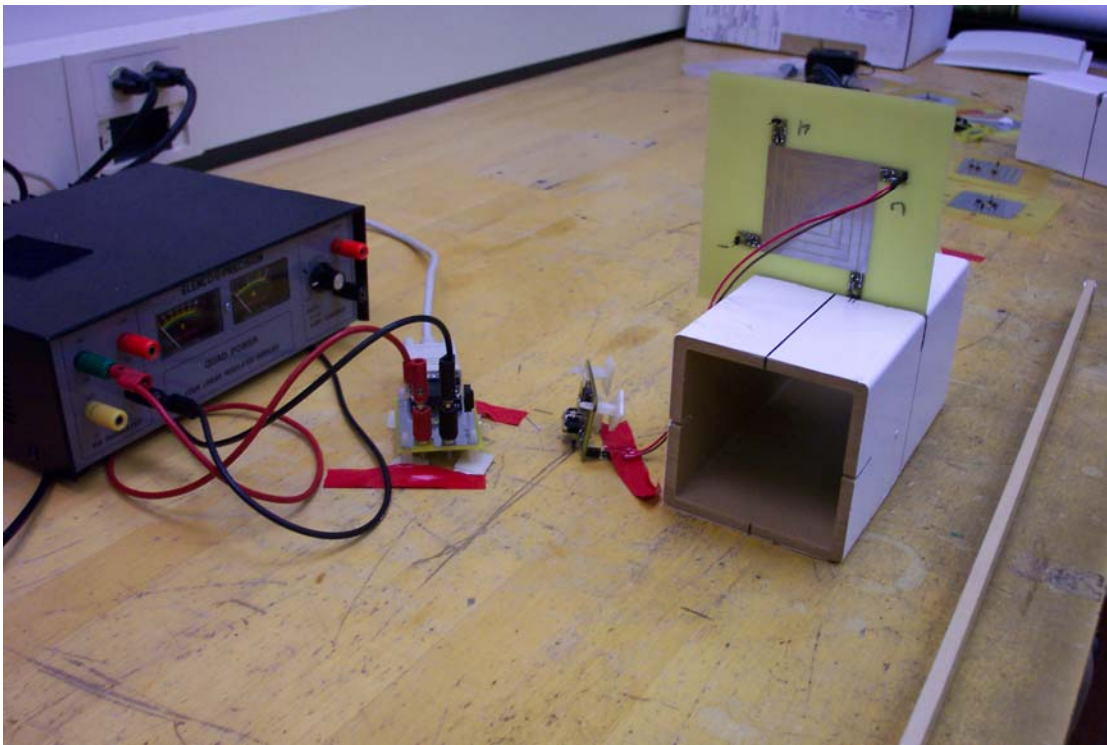


**Figure 3.1.** Sarlacc Polarization Test 1



**Table 3.13.** Sarlacc Polarization Test 1

Position	Element	Voltage (mV)
Left	1	482.45
Bottom	2	29.33
Right	3	338.74
Top	4	557.72

Elements on the left, right, and top are significantly outperform the element on the bottom. The test was then repeated after rotating the Sarlacc design 90 degrees clockwise so that element number 2 was now on the left.

**Table 3.14.** Sarlacc Polarization Test 2

Position	Element	Voltage (mV)
Left	2	421.83
Bottom	3	11.24
Right	4	350.47
Top	1	498.58

Again, the elements on the left, right, and top significantly outperform the bottom. Poor soldering can be eliminated as the reason for element 2's poor performance because it now performs equally as well as the other elements from Test 1. The elements on the bottom and the right perform the worst; these elements are also the ones for which the wires are stretched the

farthest across the antenna being tested. Wires can also act as antennas and in this case would appear to be interfering with the measurements.

As a final test to determine whether or not this assertion is true, Sarlacc was left stationary and the transmitting antenna was rotated. All measurements were taken from element number 1 positioned on the left.

**Table 3.15.** Sarlacc Polarization Test 3

Orientation	Voltage (mV)
1	544.52
2	472.18
3	529.86
4	476.58

From these results it appears that the transmitter is indeed circularly polarized and that the assertion of wires interfering with the measurements is justified.

### 3.3 EVALUATION

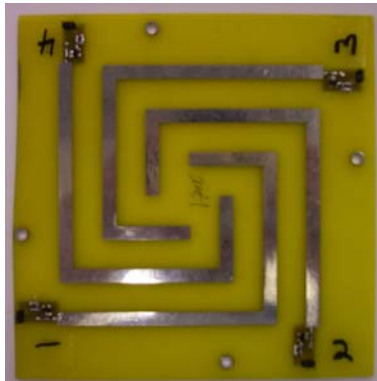
Presented below are all of the results of the measurement tests for the Minhong design. Results for the other four designs are in Appendix A. In addition, the four symmetrical designs follow the same patterns that can be observed by looking at the results from one of the designs. These conclusions are discussed following the tables. As the Uroboros design is the only non-

symmetrical antenna there is nothing to compare it too and the lack of pattern in its results make it difficult to draw conclusions. Therefore its results are simply placed in Appendix A.

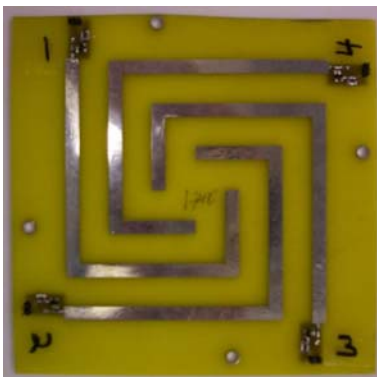
**Table 3.16.** Element Voltages Linear Polarization Position 1 – Minhong

4	3
1	2

Antenna	Voltage (mV)
1	892.55
2	58.17
3	445.30
4	593.89



**Table 3.17.** Element Voltages Linear Polarization Position 2 – Minhong

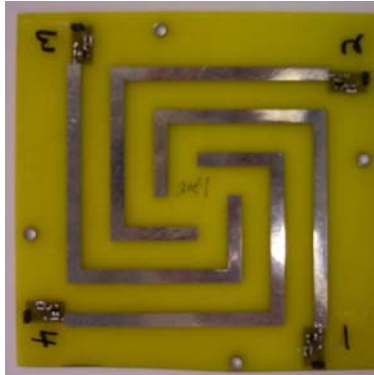
		Antenna	Voltage (mV)	
1	4	1	651.57	
		2	842.20	
2	3	3	55.23	
		4	408.64	

**Table 3.18.** Element Voltages Linear Polarization Position 3 – Minhong

Antenna	Voltage (mV)
1	442.63
2	660.86
3	783.06
4	143.71

**Table 3.19.** Element Voltages Linear Polarization Position 4 – Minhong

		Antenna	Voltage (mV)
3	2	1	207.74
		2	458.49
4	1	3	663.79
		4	857.36



By comparing the tables, one can see that the voltage is highly dependant on the elements location (orientation). The bottom left performs the best and the bottom right performs the worst. There are four distinct voltage levels that an element passes through as it is placed in each orientation, and across the elements the voltage levels in each position are similar. The bottom left being in the range of ~780-900mV, the top left ~590-660mV, the top right ~410-460mV, and the bottom right ~55-210mV. As all of the elements contain the same matching circuit and are symmetrical around the center, one would expect the voltages to be grouped in sets of two, due to the linear polarization of the antenna. As the only difference between the antennas is the wires

connecting them, it would appear that they are negatively impacting the poorly performing positions. The worst performing positions have the wires crossing in front of the antenna board; in the best performing positions the wires are hardly present at all. Figure 3.2 through Figure 3.5 below show the four different possible wire connections.

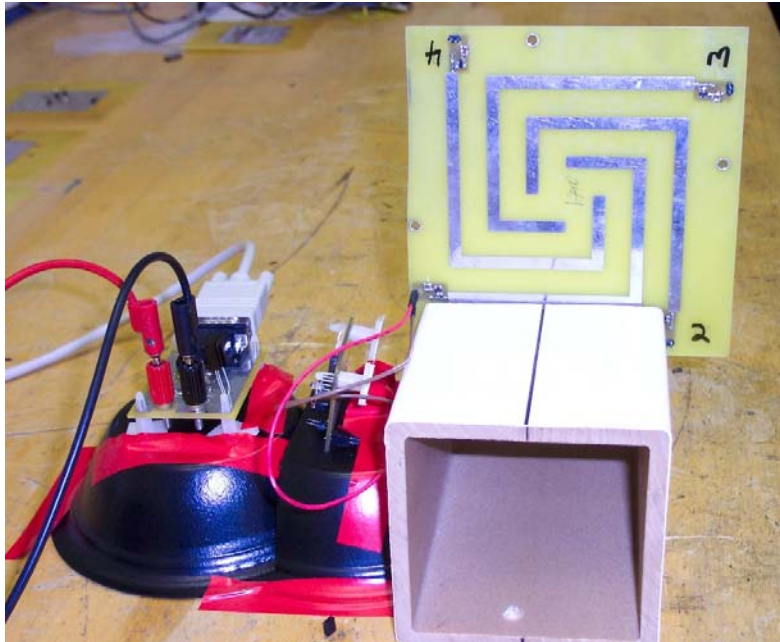


**Figure 3.2.** Wire Connection – Bottom Left

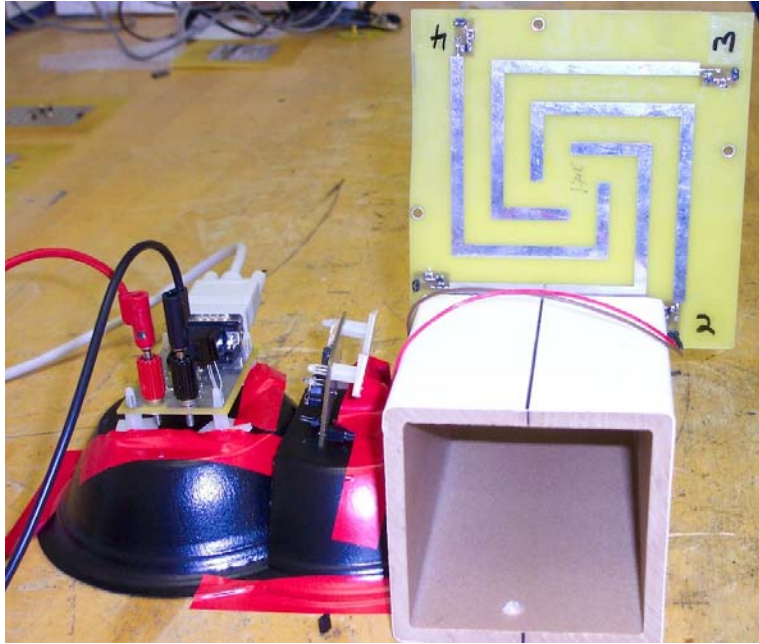


**Figure 3.3.** Wire Connection – Bottom Right

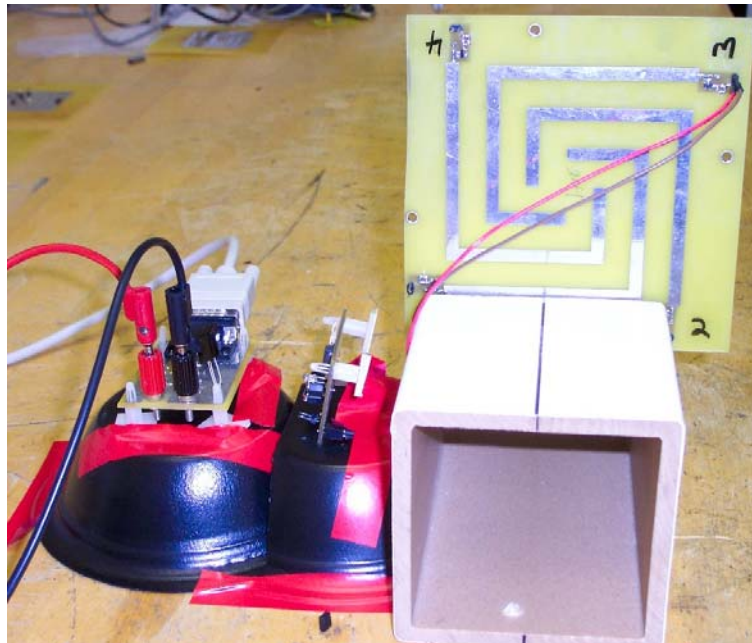


**Figure 3.4.** Wire Connection – Top Right

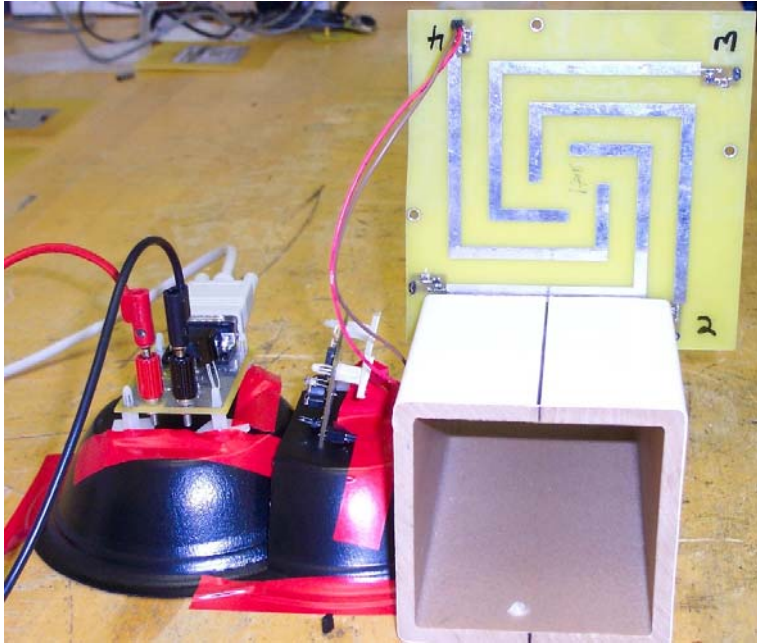
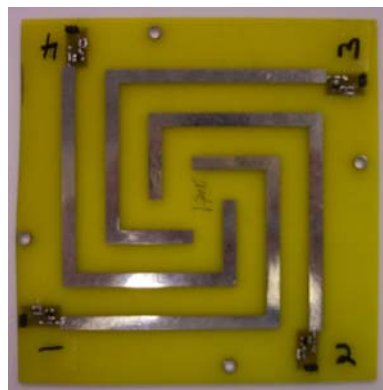



**Figure 3.5.** Wire Connection – Top Left

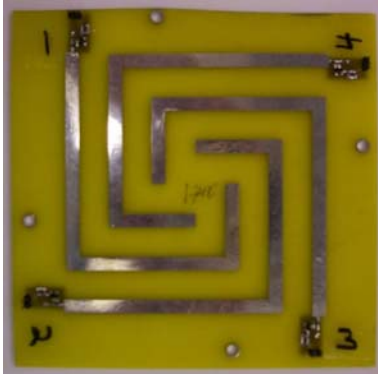
The following tables contain the results for the Minhong design using the circularly polarized antenna.

**Table 3.20.** Element Voltages Circular Polarization Position 1 – Minhong

		Antenna	Voltage (mV)
4	3	1	639.84
		2	606.60
1	2	3	21.51
		4	298.17



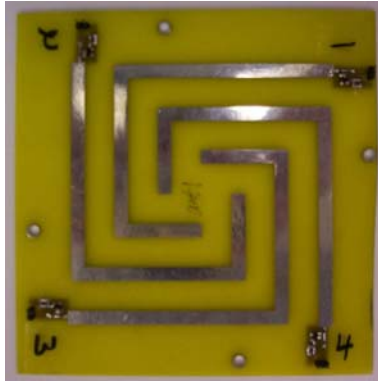
**Table 3.21.** Element Voltages Circular Polarization Position 2 – Minhong

		Antenna	Voltage (mV)	
1	4	1	349.00	
		2	618.82	
2	3	3	658.90	
		4	60.12	

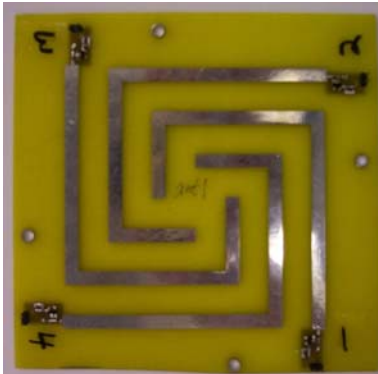
**Table 3.22.** Element Voltages Circular Polarization Position 3 – Minhong

2	1
3	4

Antenna	Voltage (mV)
1	164.73
2	414.01
3	553.32
4	621.75

| 1 | 164.73 |
2	414.01		
3	553.32		
	4	621.75	

**Table 3.23.** Element Voltages Circular Polarization Position 4 – Minhong

		Antenna	Voltage (mV)	
3	2	1	622.73	
		2	120.73	
4	1	3	287.90	
		4	636.91	



In this case the results should be close for all four elements in all orientations, because the transmitter is now circularly polarized and the antenna elements are symmetrical. This again implies that the wires are interfering with the measurements. One observation is that the worst performing location has changed. It is surmised that this is caused by the wires interacting differently with the circularly polarized field than with the previous linearly polarized field.

With the wires affecting the measurements, in order to compare the different designs, only the bottom left voltage reading will be taken into account. This is done because the wires had the least interference with this measurement, and in all designs it was the best performing location. When viewed in this fashion the designs rank as follows from most voltage to least for the linearly polarized transmitter: Minhong, Sarlacc, Oculus, Uncenter. For the circularly polarized transmitter, the ranking is: Sarlacc, Minhong, Oculus, Uncenter. An important note, both the Sarlacc and Oculus designs increased their voltage when using the circularly polarized transmitter as compared to the linearly polarized case, while the Minhong and Uncenter designs decreased their voltage. It is conjectured that the close proximity of the antenna elements in the Sarlacc and Oculus design allows the elements to interact with each other constructively when they are all energized. Both of those designs also look like a single square of metal and may behave more like a square patch antenna than the Minhong and Uncenter designs which are more spread out and open.

The distance measurements were done with the same configuration used for matching the antennas; a 0.5W 915MHz continuous wave source. Again data were collected with both a linear and circular polarized transmitter, and both tables are shown below.

**Table 3.24.** VPM Distances – Linear Polarization

Design	Distance (cm)
Minhong	94.7
Uncenter	28.0
Sarlacc	15.5
Oculus	27.1
Uroboros	~2.4v @ 0cm

**Table 3.25.** VPM Distances – Circular Polarization

Design	Distance (cm)
Minhong	48.1
Uncenter	~4.9v @ 0cm
Sarlacc	36.1
Oculus	36.2
Uroboros	~2.4v @ 0cm

The fact that the distances for the linear polarization differ greatly from those in Section 0, illustrates how large of an effect the soldered wires, connecting the antenna elements in series, have on the results. One item of note is that the Minhong design performs the best in all three tables and is therefore likely the best performing design in this test despite variations in soldering. When comparing the results of the linear and circular polarization tests, it is obvious that the Minhong and Uncenter designs performed worse when using the circularly polarized

antenna, while the Sarlacc and Oculus designs performed better. As with the individual element tests, these results indicate that using a circularly polarized antenna creates positive interference in the two antenna designs that closely resemble square patch antennas, while the more spread out designs suffer a negative impact. The precise nature of these interferences and current interactions is beyond the scope of this thesis, but would be an enlightening extension for future work. As a conjecture, it is felt that the actual distance may play a crucial role due to the effects of phase cancellation [3, 4]. This is the interactive conductor effect used to focus RF energy in reflectors [5].

The original Minhong results were achieved for a less robust orientation set of experiments, i.e. primarily focused on the cumulative energy harvested as opposed to individual antenna orientation performance. Thus, it was possible to use a single wireless Infra Red transmitter as a part of the Virtual Power Meter. However, the calibration of a measurement system of four such devices was problematic and thus would introduce numerous uncertain measurements. Thus, the wired auxiliary methodology was chosen which involved longer wire than the original Minhong experiments [1].

Thus, the wires were used initially with the caveat that their impact on the experiment would be evaluated. The effect has been noted, and an alternative is elaborated in Section 4.0 .

## **4.0 RFID TAGS**

Due to uncertainty about the effects of the numerous wires required to take measurements, a higher quality measurement mechanism was desired. This new approach involved placing Texas Instruments RFID chips onto the antenna designs and cutting a groove into the antenna to provide inductance to cancel out the capacitance of the chip. Two different structures were tried for the RFID chip used; a loop and a strap as shown in Figure 4.1 and Figure 4.2 respectively.



**Figure 4.1.** TI Loop



**Figure 4.2.** TI Strap

In this way the need for wires would be removed and chip operation as a function of distance would serve as the metric. Although maximum read distance is an appropriate comparison to the energy measurements, the relative performance of the designs could more appropriately be determined by read rate, as in many current applications the distance between reader and tag is relatively small. In the general RFID context, read rate is the percentage of times the tag is read versus the total number of attempts.

## **4.1 SIMULATION**

There are two methods by which the TI loops can be attached to the antennas, 1) Direct Connection (where the metal of the loop touches the metal of the antenna element) and 2) Capacitive Coupling (here the loop is turned over so that the PET plastic prohibits the two metals from touching). Direct Connection was investigated first. To test if this is even possible, an extra board with the Minhong design was cut with a Dremel tool. The groove was slowly lengthened, increasing the inductance, until the TI chip would read. Note that a small amount of parasitic capacitance may also be introduced, but this capacitance would be small when

compared with the inductances created. The net result is an inductive effect. Figure 4.3 below shows Minhong board with cut grooves.

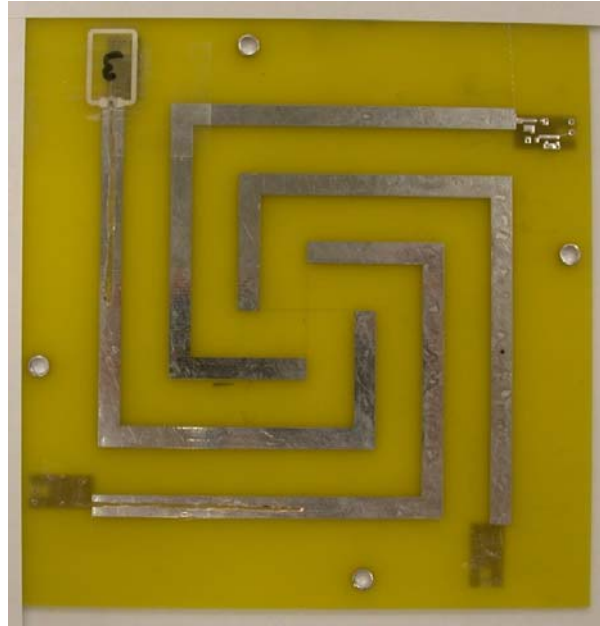


**Figure 4.3.** Minhong Board Cut with Dremel

With this basic conceptual test accomplished, further tests were conducted in which the loop was cut off and only the chip (with little metal wings for connection) was attached to the antenna. This would be beneficial through the obvious reduction in size, and also keep overlaps from occurring in the Oculus design with its compact center. However, without the extra loop the matching became extremely sensitive and imprecise. This concept for connecting the chip to the antenna was abandoned.

Once it was shown that this method, with the loop, would work, simulations were conducted in Ansoft HFSS. The Minhong design was created as a perfect conductor, the FR4 PCB material was added, and the whole entity was surrounded by an air box with sides one and a half wavelengths long. Figure 4.4 below shows the simulation environment

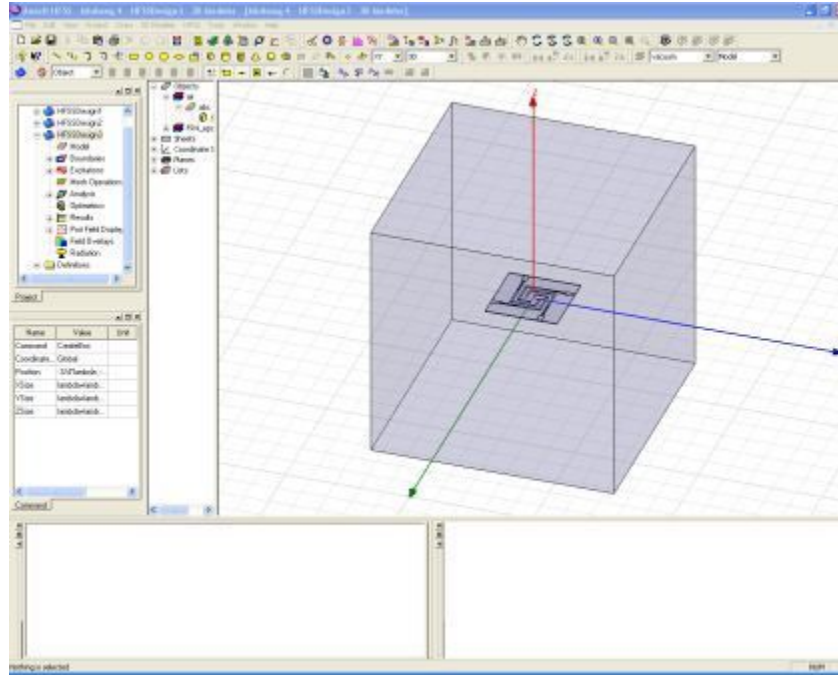


**Figure 4.4.** Ansoft HFSS Simulation Environment

The series impedance of the TI chip was known to be  $33 - j112$  [5]. However, in the connection to be used, the chip would be in parallel with the inductor and so the series impedance was converted to parallel impedance using the following equations from [7].

$$R_p = \frac{R_s^2 + X_s^2}{R_s} = 413$$

$$X_p = \frac{R_s^2 + X_s^2}{X_s} = -j121.72$$

In this case the real part of the impedance was ignored as this would require fundamental changes to the antenna design to match, and it was desired to keep the antennas in the same shape with the obvious exception of the groove. The groove length was therefore adjusted and simulations run until the reactance was close to  $+j121.72$ . Below, Figure 4.5, illustrates the

Minhong design with its final groove size, and Table 4.1 illustrates the lengths and simulated reactance, with bold numbers designating the matched length.

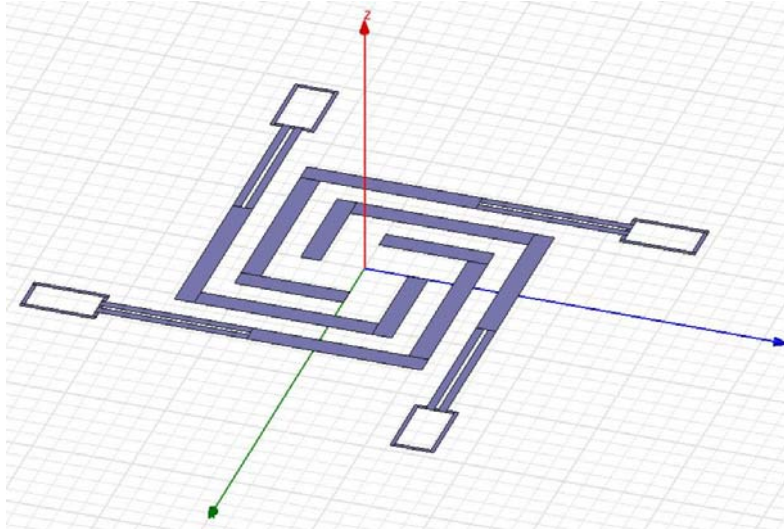


**Figure 4.5.** Minhong Design in Ansoft HFSS

**Table 4.1.** Simulated Minhong Impedance

Slot Length (mm)	Reactance
26	82.32
30	92.36
34	104.77
40	129.92
39	124.32
<b>38</b>	<b>121.31</b>



When done with the Dremel, the length was measured as 45mm, but this difference is assumed to be caused by the non-uniform, non rectangular nature of the hand cutting. The other antenna designs were also modeled in HFSS and are shown in Figure 4.6 - Figure 4.9. The Uroboros design was modeled and simulated; however, due to its lack of symmetry and interactions between each antenna element, they could not all be matched at the same time as matching one element would cause another to no longer have the proper matching.

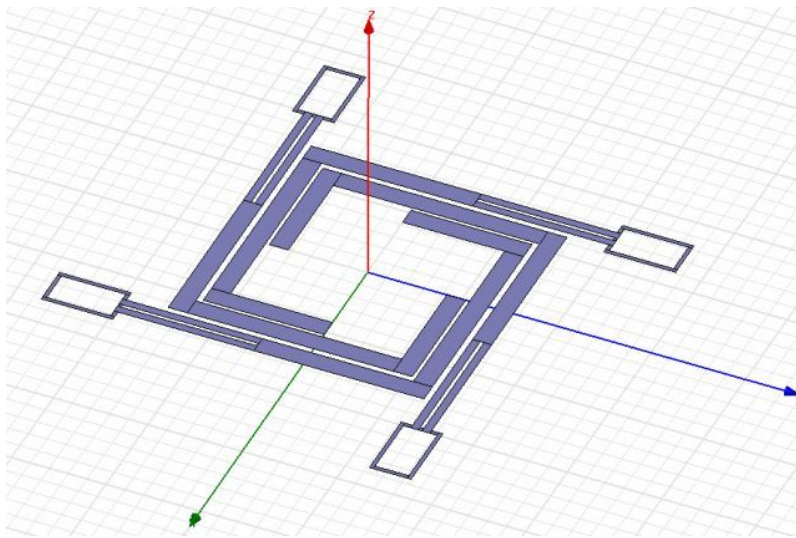


**Figure 4.6.** Uncenter Design in Ansoft HFSS

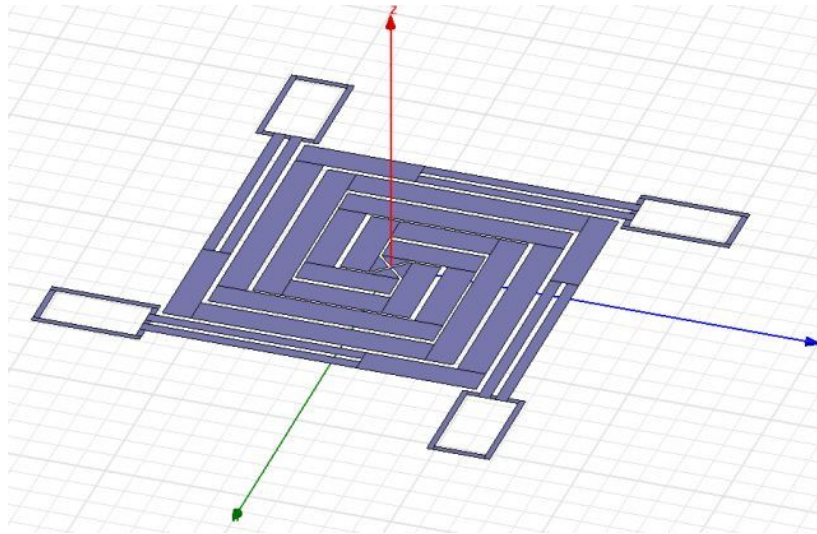


**Figure 4.7.** Sarlacc Design in Ansoft HFSS

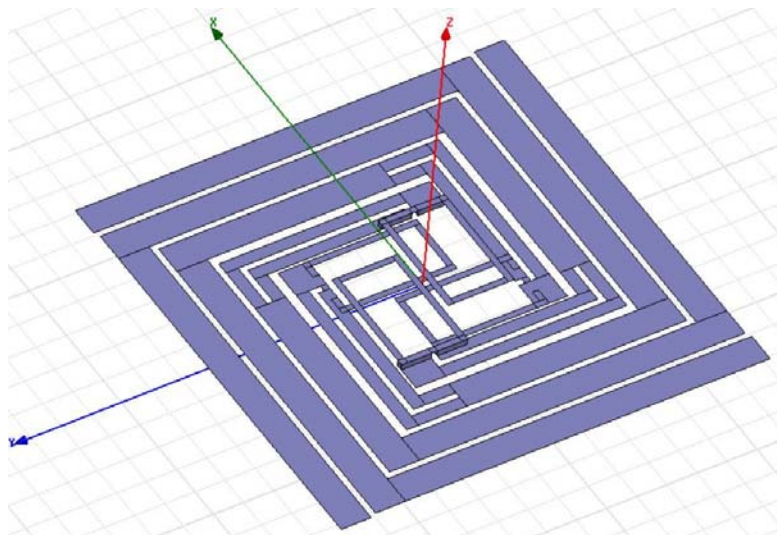


**Figure 4.8.** Oculus Design in Ansoft HFSS

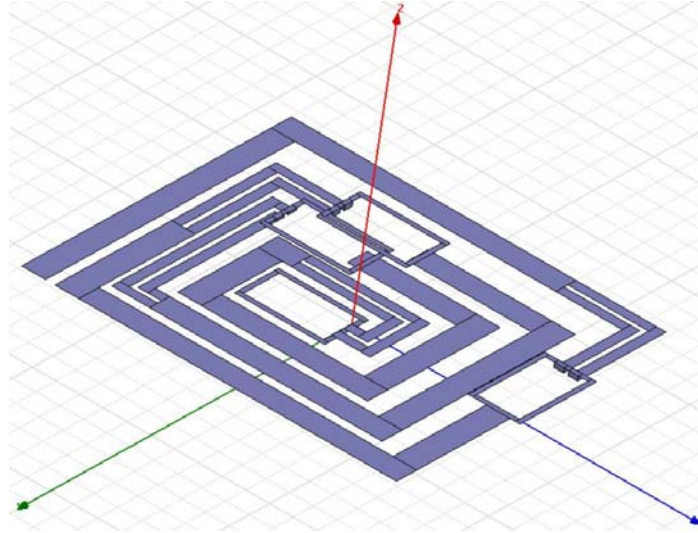


**Figure 4.9.** Uroboros Design in Ansoft HFSS

## **4.2 DIRECT CONNECTION**

Once the proper length was determined, the designs were fabricated using Express PCB. When the actual boards arrived with grooves, the Minhong design worked with a minimum of effort once a hole was made for the chip to rest in so that the contacts were flush, and it was securely taped down it would respond in the anechoic chamber, Figure 4.10. The other two boards, Uncenter and Sarlacc, were much more difficult. In each case, a single chip worked very well but the other chips would either read poorly or not at all. Many attempts were made to resolve this issue. Holes were made larger in case the chip was not fitting flush, a conductive polymer was used to form a complete connection. None of these changes fixed the problem. As the tags performed better the less they were handled, it seems probable that the inconsistencies in read quality were caused by damaging the connection of the TI chip to the loop while attempting to align the chip with the hole in the board and ensuring that it was taped down securely to provide

a good metal connection. Although even when using new chips, a uniform level of performance could not be achieved.



**Figure 4.10.** Sarlacc Board in Anechoic Chamber

Further testing results are presented in Section 5.2 after which the connection method was changed to capacitive coupling.

### **4.3 CAPACITIVE COUPLING**

With physical connections again creating difficulties, the second method of capacitive coupling was tried to remove any dependence on metal touching metal. Going back to the old boards with

Dremel work, new grooves were cut to match the TI RFID chips which were now capacitively coupled instead of directly connected. In this case the cutout loops were simply turned over as the plastic backing provided an insulator between the loop of metal connected to the TI chip and the metal of the antenna element. Each of the designs was matched in this fashion. For the Minhong, Uncenter, and Sarlacc designs, the required groove was longer than the groove that was needed in simulation for a direct connection. The significance of this was that the boards that were already built with grooves could be reused by adding an extension made with the Dremel. This would minimize the differences between each antenna element of a given design, by minimizing the hand cut length. Figure 4.11, below, is a diagram of how the TI loop is connected for capacitive coupling. The pink rectangles are the metal, the upper rectangle is the loop, the lower lines are the antenna element, and the gray rectangle separating them is the PET. It can be seen in this diagram that the metal portions are not touching.

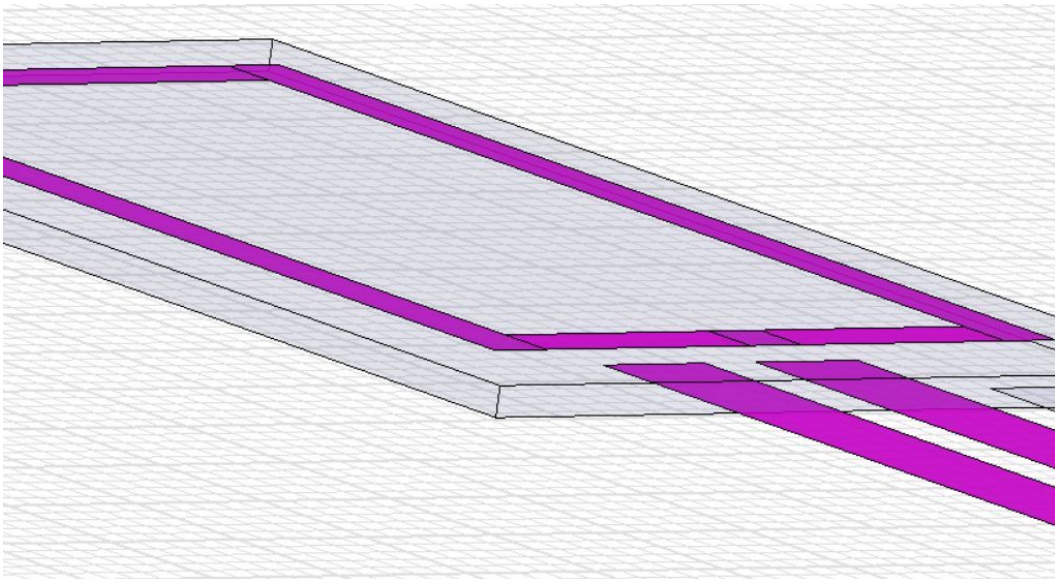


**Figure 4.11.** Diagram Showing Coupling

The Oculus board could not be matched in its current design with the loop in the center. A new board had to be built in which the groove was straight, as can be seen in Figure 4.12. In this case the loops lie on top of the other antenna elements. This type of configuration would not have been possible with the direct connection method as the metal of the loops would contact the metal of the other antenna elements and short the energy harvesting.

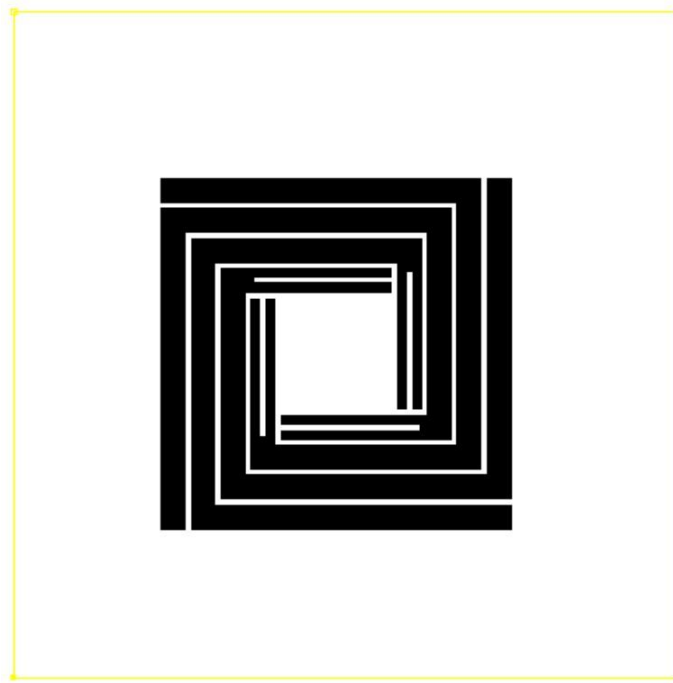


**Figure 4.12.** Oculus Coupling Layout

Using capacitive coupling, the antenna designs could not be simulated to verify that optimal matching was achieved. After adding the separation into the HFSS layout, the simulation would no longer converge and produce results. It is conjectured that the extremely narrow separation,  $76.2\mu\text{m}$ , representing the PET created too many meshing interactions for the program to properly optimize. It is possible that, with an intricate knowledge of Ansoft HFSS, the program could have been directed by the user to the sections of the design that should be



focused on or through some other means caused the result to converge. However, this knowledge being unavailable and time not permitting, the results that were verified physically, i.e. the Dremel work, were considered sufficient.

The main purpose of removing the physical connection is to simplify the connection between chip and antenna. Far less precision is required in placing the coupled loop on top of the antenna element than in making a direct connection between the two. A side effect of this is that the capacitively coupled connections outperformed the direct connections in terms of read rate during initial testing in the anechoic chamber. Figure 4.13 through Figure 4.16 show the antenna designs with TI chips connected via coupling. Notice that the end opposite the RFID chip has been elongated with a Dremel to accomplish the matching and varies slightly from element to element.

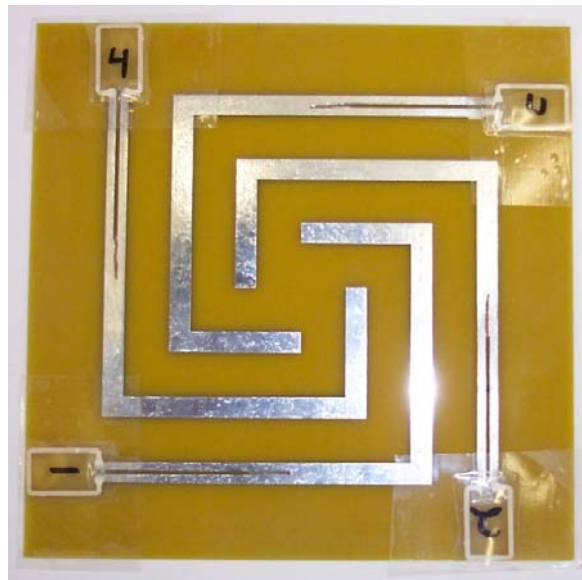


**Figure 4.13.** Minhong Design with Coupling

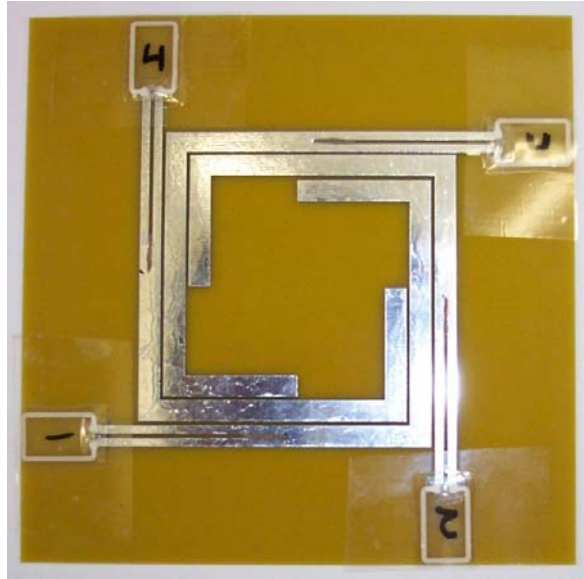


**Figure 4.14.** Uncenter with Coupling

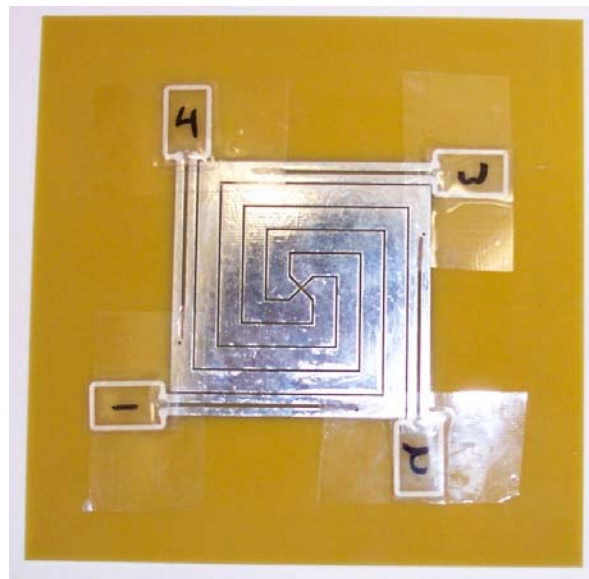


**Figure 4.15.** Sarlacc with Coupling



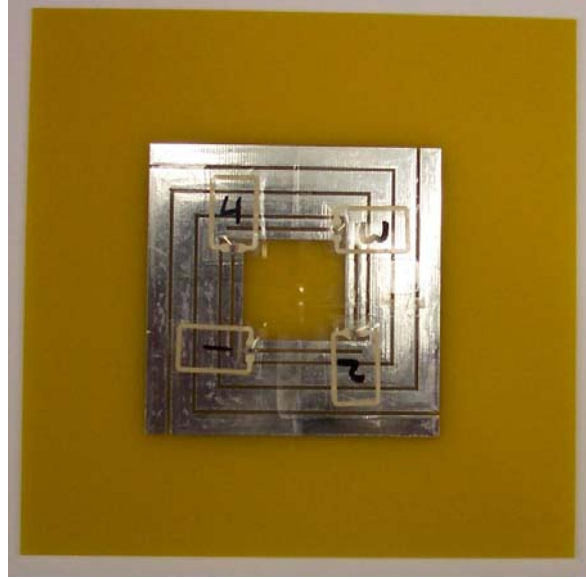


**Figure 4.16.** Oculus with Coupling

#### **4.4 EVALUATION METHODS**

The designs were compared in two ways. First, the read rates of all four antenna elements for each design will be recorded using a linearly polarized antenna and then with a circularly polarized antenna. With each polarization, the proposed design rotated 90 degrees each of three times so that each antenna element is measured in one of the four possible positions.

Second, the maximum read range is calculated by measuring the minimum power required to read the tags at a known distance and using the simplified Friis transmission equation [8]. This will be done with both the linearly and circularly polarized antennas and at a frequency of 915.1MHz.

Equation 4.1 is the Friis equation with appropriate values for the maximum read distance  $R$ , in meters.

$$\frac{P_r}{P_{t \max}} = G_t G_r \left( \frac{\lambda}{4\pi R} \right)^2 \quad 4.1$$

Equation 4.2 is for the test setup with separation  $d$ , also in meters.

$$\frac{P_r}{P_{t \min}} = G_t G_r \left( \frac{\lambda}{4\pi d} \right)^2 \quad 4.2$$

Canceling common terms and rearranging these expressions yields

$$R = d \sqrt{\frac{P_{t \max}}{P_{t \min}}} \quad 4.3$$

Where  $P_{t \max}$ , which is governed by the FCC, can be rewritten as  $EIRP / G_t$

$$R = d \sqrt{\frac{EIRP}{P_{t \min} G_t}} \quad 4.4$$

Where  $d$  is the known distance,  $P_{t \min}$  is the minimum power required to read at that distance,  $G_t$  is the transmitting antenna gain, and  $EIRP$  is the Equivalent Isotropic Radiated Power, which in this case is a maximum of 4W. With an RFID reader the gain of the linearly polarized antenna is 6dBi, and the gain of the circularly polarized antenna is 8dBic. The tests is performed using the setup shown in Figure 4.17. The tests could not be performed in the anechoic chamber because the antenna in the chamber is linearly polarized (forcing the circularly polarized tests to be done outside) and some of the antenna designs could not be read at the distance provided in the chamber and could not be placed closer due to the delicate nature of the RF absorbing cones.

For these reasons the tests were run in open air with some RF absorbing foam placed around them.

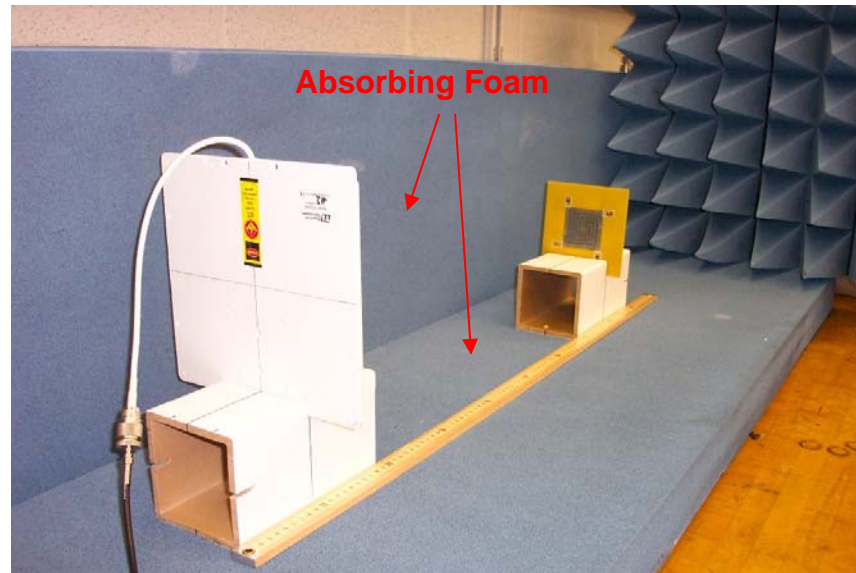


**Figure 4.17.** Max Read Range Setup

Also, because the device used in the tests is an actual Gen2 RFID reader, there are limits on the available power outputs. This created a small problem in that all of the antennas could not be tested at the same separation. One of the antenna designs needed to be very close to the transmitter in order to read, but a different, better performing design, would read at the lowest power setting at that same distance. As the maximum read range equation is based upon the minimum power and the tag read at the lowest power setting, it is unknown what the minimum power actually was. Therefore, each antenna was placed at a unique separation for testing, which was as far away as possible while still providing consistent results in order to minimize any near field effects. Using the FCC definition, the far field begins at  $R$  given by Equation 4.5, where  $D$  is the maximum dimension of the antenna and  $\lambda$  is the wavelength [9].

$$R = \frac{0.6D^2}{\lambda} \quad 4.5$$

For this particular setup

$$D = 0.26m$$

$$\lambda = 0.327m$$

$$R = 0.206m$$

To run the test, a Visual Basic program was used to increase the power output of the reader in steps and attempt to read the tag at each power level. The power level when the tag is first read is stored as the minimum turn on power. After attempting each read there is a wait of 5 seconds built into the program. This is done to ensure a consistent non-energized starting point. According to the EPC Global Gen2 specification, tags are required to maintain session states for a persistence time in some cases as long as 5 seconds [10]. This implies that the tag must be retaining power for that long. If the program did not wait 5 seconds between reads, allowing the stored power to dissipate, it is possible that the tag could incrementally store power and read at a lower power level than is actually required to turn the tag on.

## 5.0 RFID TAG RESULTS

### 5.1 SIMULATION

Contained here are the results of the simulation data for the Uncenter, Sarlacc, and Oculus board. Tabulated below are the data from the simulation runs for each antenna, showing slot length and reactance. Here again the bold line indicates the length which provided the best matching and was subsequently used in building the antenna designs for direct connection.

**Table 5.1.** Uncenter Simulation Results

Slot Length (mm)	Reactance
<b>38</b>	<b>122.08</b>
37	120.88

**Table 5.2.** Sarlacc Simulation Results

Slot Length (mm)	Reactance
6	23.09
16	53.02
30	93.22
37	118.21
<b>38</b>	<b>122.08</b>

**Table 5.3.** Oculus Simulation Results

Slot Length (mm)	Reactance
20	72.93
28	104.00
36	131.27
34	118.93
<b>35</b>	<b>122.9</b>

An important observation from these results is that the Minhong, Uncenter, and Sarlacc designs all had the same slot length for matching, and the Oculus was also close to this value. This was not the case during the hand matching where each of the designs required different capacitor and inductor values in the matching circuit for optimum energy harvesting. This could imply that matching the antennas by hand incorporated undesired errors.

## 5.2 DIRECT CONNECTION

These results are continued from Section 4.2 examining the direct connection method. The testing was moved outside of the anechoic chamber so that a circularly polarized antenna could be used to determine if performance would improve. Figure 5.1 shows the setup for this test.

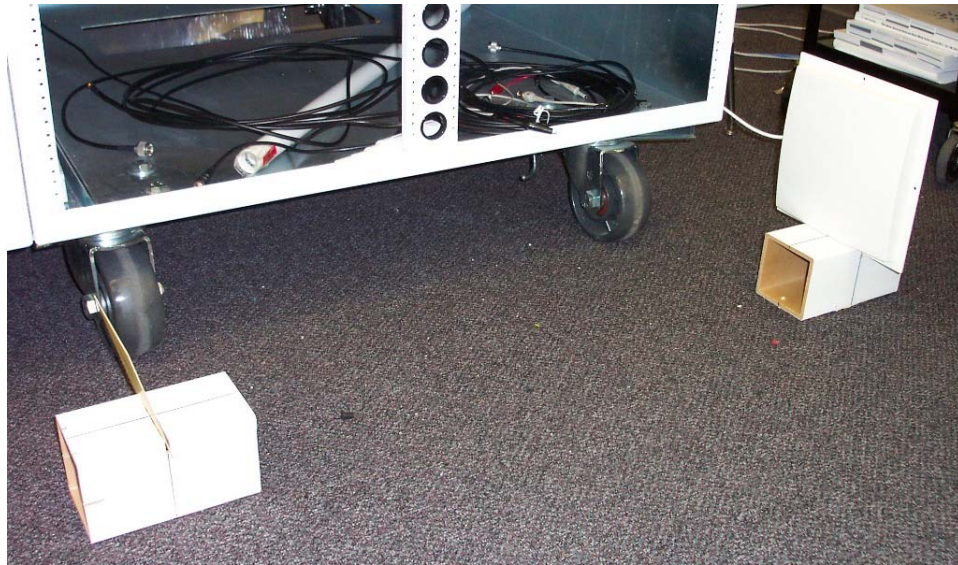


**Figure 5.1.** Circularly Polarized Sarlacc Test

As the antennas could now be placed closer together than in the anechoic chamber, the other RFID chips began to read, although at a lower read rate than those that worked in the anechoic chamber. This asymmetric performance of symmetric antennas was reminiscent of the previous work with the VPM voltage measurements. In order to test this theory, the read rate of the Sarlacc design was recorded for each antenna element, and then rotated 90 degrees and repeated until each antenna element had been tested in each location. Tables are shown below with a figure for reference indicating the location of each element.

**Table 5.4.** External Circular Polarization Position 1 – Sarlacc

4	3
1	2

Element	Read Rate
1	60
2	25
3	65
4	25

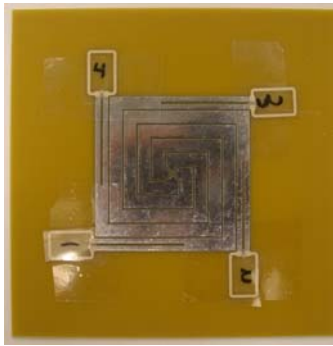


**Table 5.5.** External Circular Polarization Position 2 – Sarlacc

		Element	Read Rate	
1	4	2	50	
		3	60	
2	3	4	45	
		1	30	

**Table 5.6.** External Circular Polarization Position 3 – Sarlacc

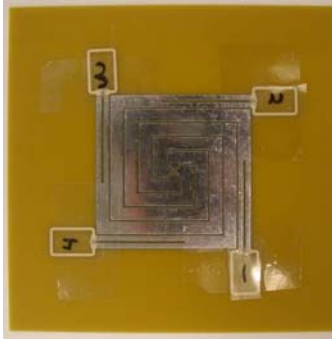
		Element	Read Rate	
2	1	3	60	
		4	45	
3	4	1	45	
		2	20	



**Table 5.7.** External Circular Polarization Position 4 – Sarlacc

3	2
4	1

Element	Read Rate
4	50
1	30
2	50
3	55

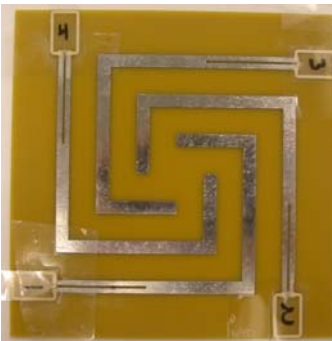
A micrograph of a square spiral antenna on a yellow substrate. The antenna is a square spiral with four leads extending to the corners, labeled 1, 2, 3, and 4. The leads are connected to small gold pads. The spiral itself is made of a dark, conductive material. The labels are small white squares with black numbers. The substrate is a uniform yellow color.

Ignoring element 3, which performs consistently independent of its orientation, the observation can be made that the antennas perform better when in the top right and lower left corners ( $>45$ ) and worse when in the top left and bottom right ( $<30$ ). This would imply that the orientation is having an effect on the antenna elements ability to harvest energy, similar to the results of the VPM when measuring voltages.

Table 5.8 - Table 5.11 show the results of the circular polarization tests using the Minhong design.

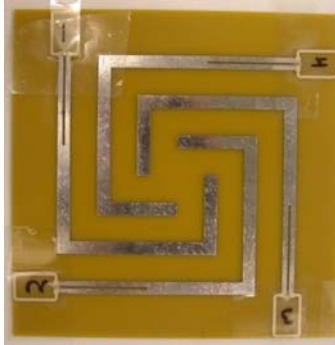
**Table 5.8.** External Circular Polarization Position 1 – Minhong

		Antenna	Read Rate
4	3	1	35
		2	50
1	2	3	50
		4	40

A photograph of a square spiral antenna printed on a yellow substrate. The antenna is a silver-colored metal trace forming a square spiral. Four small white labels with black numbers are placed at the corners of the spiral: '1' at the top-left, '2' at the bottom-right, '3' at the top-right, and '4' at the bottom-left. The spiral starts from the center and winds outwards in a clockwise direction.

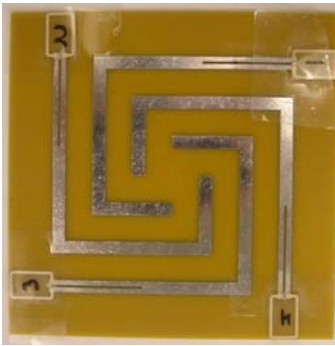
**Table 5.9.** External Circular Polarization Position 2 – Minhong

		Antenna	Read Rate
1	4	2	50
		3	60
2	3	4	45
		1	25

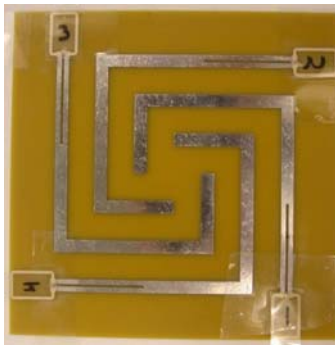
A photograph of a square spiral antenna printed on a yellow substrate. The spiral is made of a silver-colored conductive material. Four feed points are located at the corners of the square, each labeled with a number: '1' at the top-left, '2' at the top-right, '3' at the bottom-right, and '4' at the bottom-left. The spiral starts from the center and winds outwards in a clockwise direction.

**Table 5.10.** External Circular Polarization Position 3 – Minhong

		Antenna	Read Rate
2	1	3	55
		4	45
3	4	1	35
		2	40

A photograph of a square spiral antenna printed on a yellow substrate. The spiral is made of a silver-colored conductive material. Four feed points are located at the corners of the square, each labeled with a number in a small black box: '2' at the top-left, '1' at the top-right, '3' at the bottom-left, and '4' at the bottom-right.

**Table 5.11.** External Circular Polarization Position 4 – Minhong

		Antenna	Read Rate	
3	2	4	50	
		1	30	
4	1	2	50	
		3	50	

In contrast to the Sarlacc design results, the antenna elements in the Minhong design perform about the same regardless of their position, especially numbers 2 and 4, likely due to better direct connections.

### **5.3 CAPACITIVE COUPLING**

The capacitive coupling connection method did not suffer from the connection issues of the direct method, and so was used for evaluating the designs. The methods for the two tests were outlined in Section 4.4.

#### **5.3.1 Read Rate**

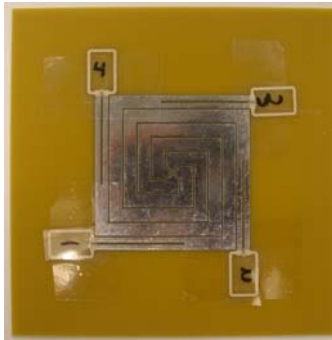
The read rate test was performed with both a linearly polarized and circularly polarized antenna. In both cases a SamSys RFID reader was placed in continuous read mode at its maximum power of 320 tenths of dBm. For the linear polarization, a distance of 50cm was used because it was the maximum distance all designs, except Minhong, would function and it was well beyond the beginning of the far field. For the circular polarization, it was shortened to 40cm as that was a better illustration of the operation of all four antenna elements. Also, for comparison, the TI RFID tag from which the loops were cut was also measured under the same conditions. At neither distance could the Minhong design be read. Therefore, the results of the Sarlacc design will be examined here with results for the other antennas placed in Appendix B.

It is not believed that the poor performance of the Minhong design stems from bad matching. Both the Sarlacc and Uncenter boards were hand matched with a Dremel on the first

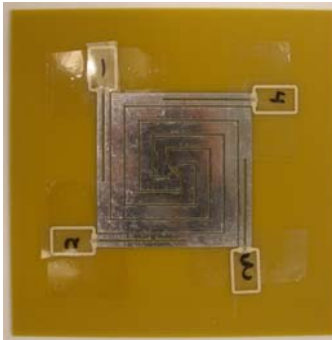
try, and performed very well. However, seven different attempts were made to match the Minhong design due to its abysmal performance. Eventually the best performing of the seven attempts was used for testing.

The following tables show the read rates for the Sarlacc design using the linearly polarized transmitter. These values are mostly as would be expected. Two tags are read for each orientation due to the linear polarization of the transmitting antenna. All three of the antennas followed this structure except in position 3, where three antenna elements were read.

**Table 5.12.** Read Rate Linear Polarization Position 1 – Sarlacc

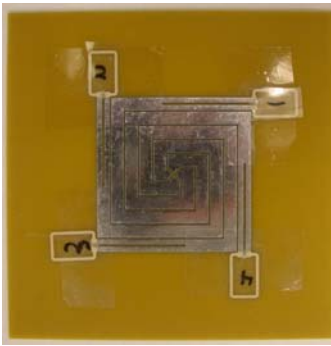
		Antenna	Read Rate	
4	3	1	7.2	
		2	-	
1	2	3	9.4	
		4	-	

**Table 5.13.** Read Rate Linear Polarization Position 2 – Sarlacc

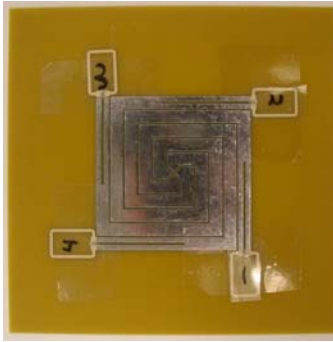
		Antenna	Read Rate	
1	4	1	-	
		2	7.4	
2	3	3	-	
		4	9.5	

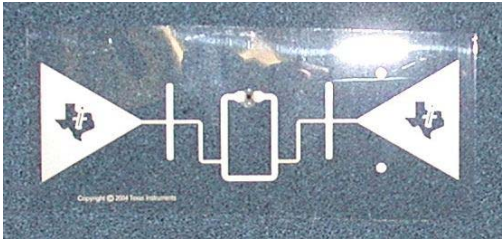
**Table 5.14.** Read Rate Linear Polarization Position 3 – Sarlacc

		Antenna	Read Rate
2	1	1	5.2
		2	-
3	4	3	9.2
		4	0.6

**Table 5.15.** Read Rate Linear Polarization Position 4 – Sarlacc

<table><tr><td>3</td><td>2</td></tr><tr><td>4</td><td>1</td></tr></table>	3	2	4	1	Antenna	Read Rate
	3	2				
	4	1				
	1	-				
	2	6.6				
3	-					
4	11.5					

**Table 5.16.** Read Rate Linear Polarization – TI Tag

Position	Read Rate	
Horizontal	-	
Vertical	20.0	

The Uncenter design had three tags read in position 3 rather than the expected 2, as well. In the case of the Sarlacc, due to the low read rate, it is likely a random event caused by the open air nature of the test. However, for the Uncenter design the read rate is comparable to the other

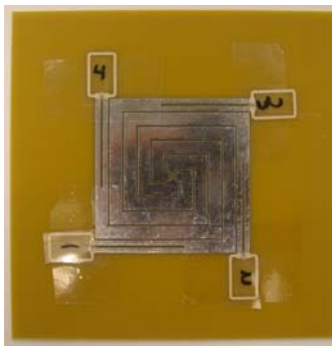
two tags that are expected to be read. One possible reason is that the centers of the transmitter and testing antennas were not aligned and that variations in the manufacturing process of the TI tag caused this particular chip to be better connected to the loop, allowing it to procure the necessary power to read from a non ideal position.

The following tables contain the read rates using the circularly polarized transmitting antenna. In this test all four antenna elements are being read at the same time, although not at the same read rate.

**Table 5.17.** Read Rate Circular Polarization Position 1 – Sarlacc

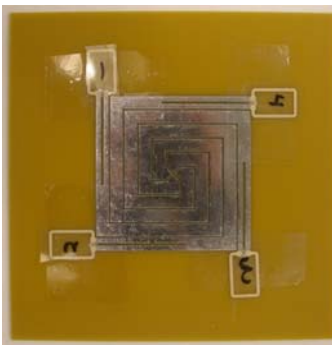
		Antenna	Read Rate
4	3	1	5.0
		2	4.8
1	2	3	3.0
		4	4.7

		Antenna	Read Rate
4	3	1	5.0
		2	4.8
1	2	3	3.0
		4	4.7

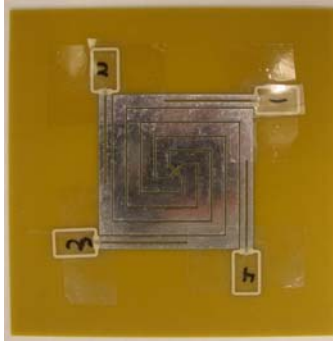


**Table 5.18.** Read Rate Circular Polarization Position 2 – Sarlacc

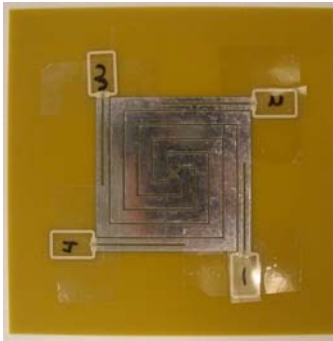
		Antenna	Read Rate
1	4	1	-
		2	4.5
2	3	3	1.6
		4	10.1



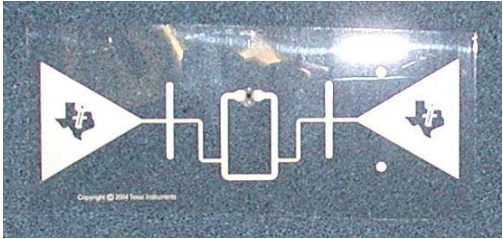
**Table 5.19.** Read Rate Circular Polarization Position 3 – Sarlacc

		Antenna	Read Rate	
2	1	1	4.3	
		2	5.6	
3	4	3	3.2	
		4	4.6	

**Table 5.20.** Read Rate Circular Polarization Position 4 – Sarlacc

		Antenna	Read Rate	
3	2	1	0.4	
		2	2.6	
4	1	3	5.8	
		4	6.4	

**Table 5.21.** Read Rate Circular Polarization – TI Tag

Position	Read Rate	
Horizontal	19.2	
Vertical	19.5	

Under optimal conditions, these results would be expected to be roughly the same for all of the elements in all positions due to symmetry. However, there are numerous variations that

can account for the differences. As mentioned earlier variation in the TI manufacturing process can play a role. Additionally, the hand cut extensions to the grooves are all different and the tags were all taped by hand allowing for the possibility of skew. If the entire process could be better controlled, hopefully, the results would be more consistent. However, this does prove that four antennas can be placed close together while still functioning to provide power to four different RFID tags.

Comparison to the TI manufactured tag shows that, for all designs, the read rates are lower than the TI tag, but are better than half its read rate for some individual antenna elements.

### **5.3.2 Maximum Distance**

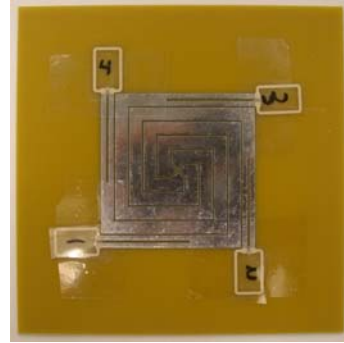
This sections details the results of the maximum read distance test. Here again the results for the Sarlacc design will be presented as the Minhong design did not perform well. In addition, the separation used in measuring the Sarlacc design was the same for both the linear and circular polarization, and the TI tag used for comparison was also measured with this separation. As stated in Section 4.3, the power was slowly increased until the tag would read and that minimum power was used to calculate the maximum possible read range. For all antenna designs the separation used is great enough to be in the far field according to the FCC definition, therefore allowing the use of the Friis equation method for calculation of maximum read range. Here also results for the other designs can be found in Appendix B.

For the Sarlacc design, the distance between it and the transmitting antenna was 70cm. The tables below present the results for the linearly polarized antenna. As in the read rate tests only two antennas will respond when using the linearly polarized transmitting antenna.

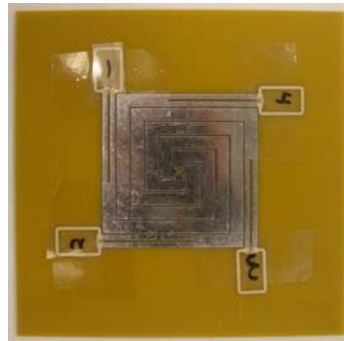


**Table 5.22.** Read Range Linear Polarization Position 1 – Sarlacc

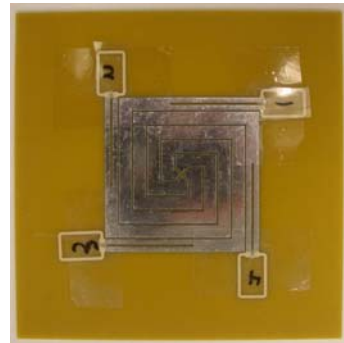
4	3	Antenna	Power (dBm)	Range (m)
		1	19.5	1.81
		2	-	Unreadable
1	2	3	20.5	1.81
		4	-	Unreadable

**Table 5.23.** Read Range Linear Polarization Position 2 – Sarlacc

1	4	Antenna	Power (dBm)	Range (m)
		1	-	Unreadable
		2	20.5	1.81
2	3	3	-	Unreadable
		4	17.5	2.28

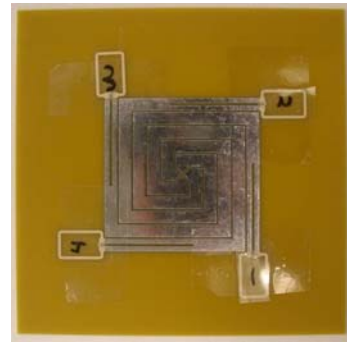
**Table 5.24.** Read Range Linear Polarization Position 3 – Sarlacc

2	1	Antenna	Power (dBm)	Range (m)
		1	20.5	1.81
		2	-	Unreadable
3	4	3	19.5	1.81
		4	-	Unreadable

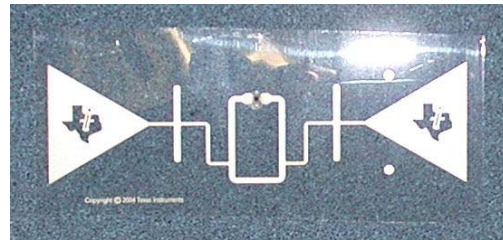


**Table 5.25.** Read Range Linear Polarization Position 4 – Sarlacc

		Antenna	Power (dBm)	Range (m)
3	2	1	-	Unreadable
		2	22	1.44
4	1	3	-	Unreadable
		4	17	2.55

**Table 5.26.** Read Range Linear Polarization – TI Tag

Position	Power (dBm)	Range (m)
Vertical	15.5	2.86
Horizontal	-	Unreadable



These results are far more consistent than the read rate results, behaving exactly as would be expected for a linearly polarized antenna with no anomalies. Comparing the Minhong, Uncenter, and Sarlacc designs it is apparent that the maximum read range increases as the antennas get closer together. In this case the Sarlacc design, which looks much like a square patch antenna, performs almost as well as the TI tag. Although the Oculus design is also similar in appearance to a square patch antenna, its performance is between that of the Minhong and Uncenter designs. It is conjectured that this is caused by the Oculus loops overlapping multiple antenna elements due to their configuration and that this interferes with optimal functioning.

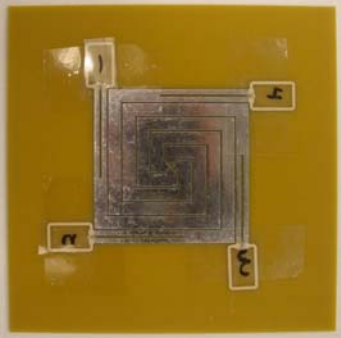
The tables below present the results for the Sarlacc design using the circularly polarized antenna. As with the read rate test, all antenna elements will respond using a circularly polarized

antenna. As before the inconsistency in range is most likely due to human error in connecting the loops to the antenna design.

**Table 5.27.** Read Range Circular Polarization Position 1 – Sarlace

<div>4      3</div> <div>1      2</div>	Antenna	Power (dBm)	Range (m)	
	1	20.5	2.47	
	2	19.5	2.47	
	3	22.5	1.97	
	4	16.5	3.92	

**Table 5.28.** Read Range Circular Polarization Position 2 – Sarlace

<div>1      4</div> <div>2      3</div>	Antenna	Power (dBm)	Range (m)	
	1	18.5	3.12	
	2	22.5	1.97	
	3	18.5	3.12	
	4	19.5	2.47	

**Table 5.29.** Read Range Circular Polarization Position 3 – Sarlacc

2	1
3	4

Antenna	Power (dBm)	Range (m)
1	21	2.21
2	20	2.47
3	21.5	1.97
4	15.5	3.92

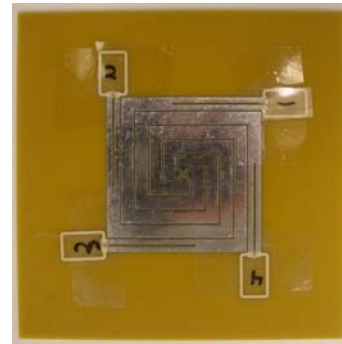


**Table 5.30.** Read Range Circular Polarization Position 4 – Sarlacc

		Antenna	Power (dBm)	Range (m)
3	2	1	18.5	3.12
		2	23.5	1.56
4	1	3	18.5	3.12
		4	18.5	3.12

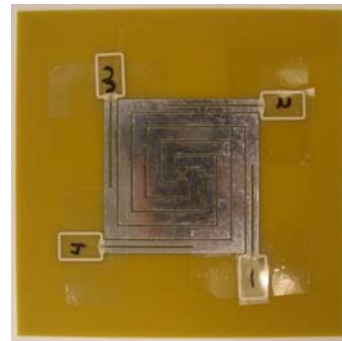
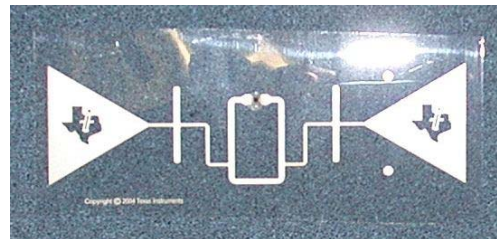


**Table 5.31.** Read Range Circular Polarization – TI Tag

Position	Power (dBm)	Range (m)
Vertical	16.5	3.92
Horizontal	14	4.94



The TI manufactured tag has again outperformed all of the designs presented here. However, there are instances where the Sarlacc design has the same read range as the TI tag.

The important result shown here is that the four tags are operating within the same space without interfering with each other. As with the voltage measurements, the Sarlacc and Uncenter boards actually improved with the use of a circular polarized antenna. This would seem to imply that close proximity is actually having a positive net effect on the energy harvesting capabilities of the design.

## 6.0 CONCLUSION

The work presented here outlines the construction, testing and evaluation of five different antenna designs with the goal of examining the affects of compressing the antennas to encompass less area. When the testing methods originally proposed [1] gave inconsistent results due to wire interference, a new method was conceived using RFID chips that not only eliminated the wires, but entirely removed a direct connection.

Table 6.1 below contains a summary of the performance of each design for those tests. To determine the rankings the best measurement (highest voltage, farthest distance, highest read rate, or longest read range) for each design regardless of orientation or element is compared. In the table ‘1’ is the best performing, ‘5’ is the worst performing, and ‘-’ indicates that no more designs were tested for read rate, because the Minhong design would not function at the distance of the test, and the Uroboros design was not made to work with the RFID tags.

**Table 6.1.** Summary of Results

Rank	Voltage		Distance		Read Rate		Read Range	
	Linear	Circular	Linear	Circular	Linear	Circular	Linear	Circular
1	Minhong	Sarlacc	Minhong	Minhong	Uncenter	Oculus	TI	TI
2	Sarlacc	Uroboros	Uncenter	Oculus	Oculus	Sarlacc	Sarlacc	Sarlacc
3	Uroboros	Minhong	Oculus	Sarlacc	Sarlacc	Uncenter	Uncenter	Uncenter
4	Oculus	Oculus	Sarlacc	Uncenter	-	-	Oculus	Oculus
5	Uncenter	Uncenter	Uroboros	Uroboros	-	-	Minhong	Minhong

The ‘Voltage’ column of Table 6.1 and the measurements in Appendix A indicate that there is a definite improvement in the performance of the compressed designs when using a circularly polarized antenna. Although the rankings did not change significantly, the voltages of the Uncenter, Sarlacc, and Oculus designs increased, while the voltage of the Minhong design decreased. This leads to the conjecture that the close proximity of the antenna elements creates a mutually beneficial environment for energy harvesting. Further work needs to be done to model the energy fields to explore why it is beneficial and what causes it so that the design can be further optimized.

As the ‘Distance’ and ‘Read Range’ columns of Table 6.1 indicate the VPM and RFID tests show differences in the design rankings. Most notable is that the Minhong design outperformed all other designs by a significant amount in the distance test using the VPM, but performed horribly in the read range test using the RFID chips. It is possible that although the Minhong design was displaying a large voltage on the VPM, its current was small due to a highly

resistive load and, therefore, the actual power available for use by the RFID chip was much less than in the other designs. For this reason the method using RFID tags and actual RFID readers is likely more accurate as it involves real world devices and less equipment in terms of power supplies and extra circuit boards for measurements. Using the RFID chips also eliminates some of the errors introduced by human interaction. This is apparent through a comparison of the sum of the read ranges for each position of each design contained in Appendix B. With the VPM, the circuits must be hand matched, but with the RFID chips, the matching could be simulated (with a better understanding of Ansoft HFSS) allowing for a better comparison of the designs. Further work would involve performing those simulations and determining if the Minhong design still performed poorly, as well as using the VPM to determine the power generated by the designs as a way to examine the cause of this incongruity between measurement methods.

Examining the ‘Read Rate’ column of Table 6.1, there is no consistency in the rankings. Most likely this is a somewhat flawed metric. When using the SamSys software, the read rate of a tag is constantly changing, and although an effort was made to record data once the rate had stabilized, there was still some jitter involved. Another difficulty with this metric is shown in the tables of Appendix B. Here the total read rate of each orientation is recorded, and it illustrates that the read rate is essentially within the range of 15-18 percent regardless of the design, orientation, or number of tags being read. As the read rate decreases proportionately for each tag as more tags are added such that the total read rate stays roughly constant it is conjectured that the SamSys reader is in fact influencing the results in some fashion.

If a point system is now assigned to each test such that rank 1 receives 5 points and rank 5 receives 1 point, totals can be generated for each design in order to rank them for overall performance.



**Table 6.2.** Overall Design Rank

	Overall		Linear		Circular	
Design	Rank	Points	Rank	Points	Rank	Points
Sarlacc	1	29	1	13	1	16
Uncenter	2	22	1	13	3	9
Oculus	3	22	3	11	2	11
Minhong	4	20	3	11	3	9
Uroboros	5	9	5	4	5	5

From Table 6.2 the Sarlacc design performed the best across all of the tests. In addition all three of the more compact designs outperformed the Minhong design. This shows that smaller more compact antenna designs can outperform a larger spaced out design.

One of the more sobering results was that nothing ever behaves the way one would expect. Despite the use of symmetric antennas, barring the Uroboros design, and a circularly polarized antenna, neither the voltage measurements, nor the read rates, nor the read ranges were uniform. The linearly polarized antenna also suffered from this same problem. Here opposite sides would be expected to perform identically, so it was not simply a bad circularly polarized antenna. The results using the RFID chips were closer to expectation; in most cases only two antenna elements would be active at a time when using the linearly polarized antenna, where as in the voltage case, all of the antenna elements were active with varying degrees of performance. Numerous factors, as discussed earlier, caused the results to deviate from what was expected; soldering, wires, loose chips, misalignment, etc. These results show the importance of a

consistent testing environment and the need for rigorous procedures to maintain consistency and eliminate as much human error as possible.

Although there were inconsistencies and none of the proposed designs performed as well as the manufactured TI tag, there is one important result. This research shows the validity of multiple antenna elements harvesting energy with small separation between them, and that under some conditions, the performance is close to that of a manufactured tag while producing other advantages not available in a single tag. It is also significant that results were achieved using a real RFID chip, that could be read and modified, moving the results out of the theoretical space and into real world application. Future work could be performed that involves compromising the rigid rectangles used for the construction of each antenna element as another design freedom in order to create a better antenna that would be capable of matching or surpassing the manufactured TI tag.

## APPENDIX A

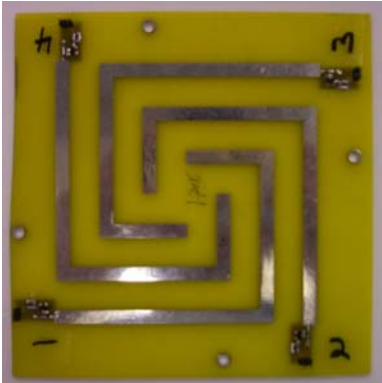
### VPM EXTENDED RESULTS

The tables below contain all of the measurements using the Virtual Power Meter for the antenna designs in multiple orientations. The Minhong design measurements are repeated here for clarity.

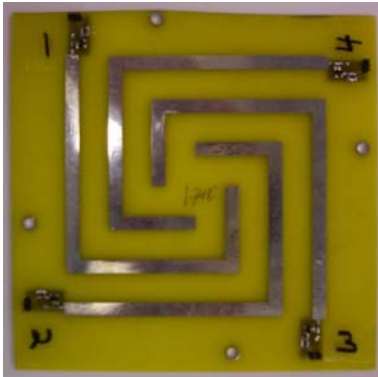
#### A.1 LINEARLY POLARIZED

##### A.1.1 Minhong

**Table A1.** Element Voltages Linear Polarization Position 1 – Minhong

		Antenna	Voltage (mV)	
4	3	1	892.55	
		2	58.17	
1	2	3	445.30	
		4	593.89	

**Table A2.** Element Voltages Linear Polarization Position 2 – Minhong

		Antenna	Voltage (mV)	
1	4	1	651.57	
		2	842.20	
2	3	3	55.23	
		4	408.64	

**Table A3.** Element Voltages Linear Polarization Position 3 – Minhong

2	1
3	4

Antenna	Voltage (mV)
1	442.63
2	660.86
3	783.06
4	143.71

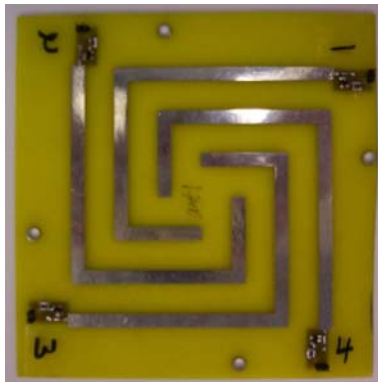
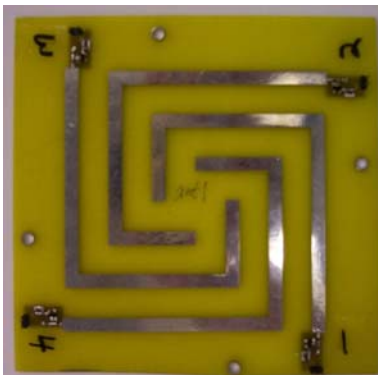


**Table A4.** Element Voltages Linear Polarization Position 4 – Minhong

		Antenna	Voltage (mV)
3	2	1	207.74
		2	458.49
4	1	3	663.79
		4	857.36

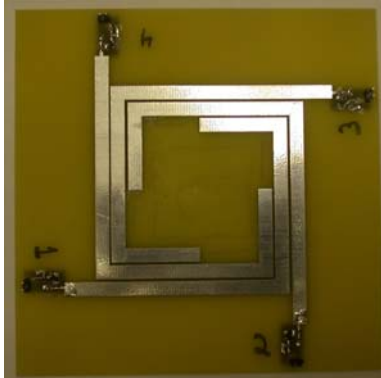


### A.1.2 Uncenter

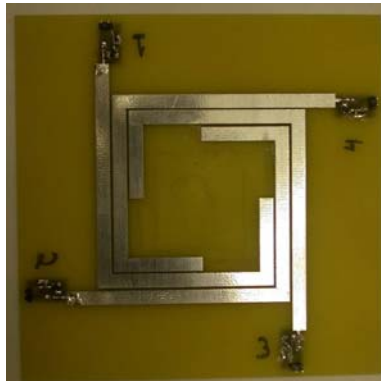
**Table A5.** Element Voltages Linear Polarization Position 1 – Uncenter

4	3
1	2

Antenna	Voltage (mV)
1	343.14
2	9.29
3	9.29
4	170.59



**Table A6.** Element Voltages Linear Polarization Position 2 – Uncenter

		Antenna	Voltage (mV)	
1	4	1	172.06	
		2	171.08	
2	3	3	14.66	
		4	58.66	

**Table A7.** Element Voltages Linear Polarization Position 3 – Uncenter

		Antenna	Voltage (mV)
2	1	1	48.88
		2	97.76
3	4	3	175.97
		4	0.00

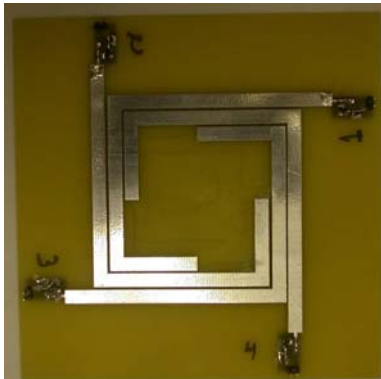
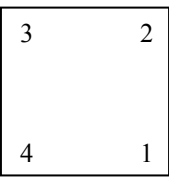
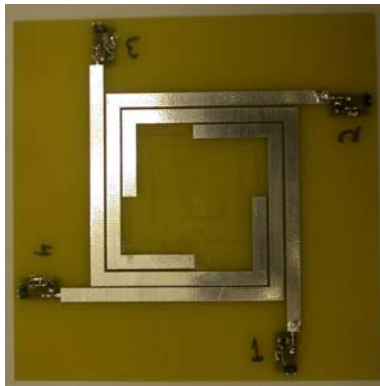


**Table A8.** Element Voltages Linear Polarization Position 4 – Uncenter



Antenna	Voltage (mV)
1	0.00
2	10.75
3	99.23
4	216.54



### A.1.3 Sarlacc


**Table A9.** Element Voltages Linear Polarization Position 1 – Sarlacc

		Antenna	Voltage (mV)	
4	3	1	770.84	
		2	847.94	
1	2	3	466.80	
		4	703.38	


**Table A10.** Element Voltages Linear Polarization Position 2 – Sarlacc

		Antenna	Voltage (mV)
1		1	742.49
		2	764.97
2		3	503.46
		4	420.86

1	4
2	3

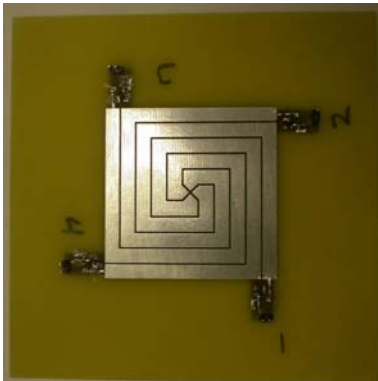


**Table A11.** Element Voltages Linear Polarization Position 3 – Sarlacc

		Antenna	Voltage (mV)	
2	1	1	468.27	
		2	740.53	
3	4	3	788.43	
		4	558.21	

**Table A12.** Element Voltages Linear Polarization Position 4 – Sarlacc


		Antenna	Voltage (mV)
3	2	1	548.92
		2	477.56
4	1	3	764.48
		4	808.48



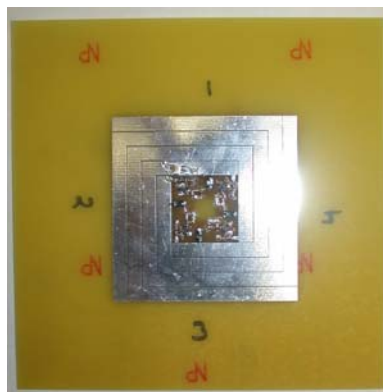
#### A.1.4 Oculus

**Table A13.** Element Voltages Linear Polarization Position 1 – Oculus


		Antenna	Voltage (mV)
4	3	1	204.32
		2	241.47
1	2	3	359.27
		4	356.82



**Table A14.** Element Voltages Linear Polarization Position 2 – Oculus

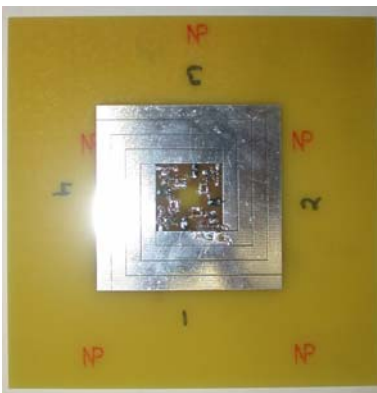
		Antenna	Voltage (mV)	
1	4	1	340.69	
		2	254.18	
2	3	3	196.01	
		4	363.67	

**Table A15.** Element Voltages Linear Polarization Position 3 – Oculus

		Antenna	Voltage (mV)	
2	1	1	353.89	
		2	381.26	
3	4	3	218.00	
		4	230.22	

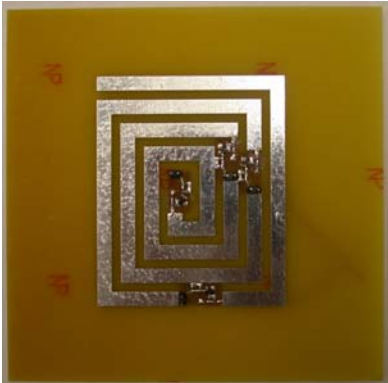


**Table A16.** Element Voltages Linear Polarization Position 4 – Oculus

		Antenna	Voltage (mV)	
3	2	1	221.43	
		2	371.49	
4	1	3	363.67	
		4	305.01	

### A.1.5 Uroboros

**Table A17.** Element Voltages Linear Polarization Position 1 – Uroboros

Antenna	Voltage (mV)	
1	507.86	
2	0.00	
3	537.19	
4	785.99	

**Table A18.** Element Voltages Linear Polarization Position 2 – Uroboros

Antenna	Voltage (mV)
1	487.82
2	264.44
3	449.70
4	329.45

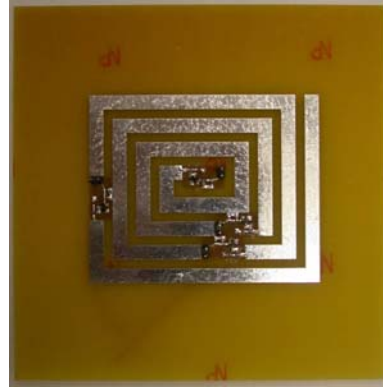


**Table A19.** Element Voltages Linear Polarization Position 3 – Uroboros

Antenna	Voltage (mV)
1	501.02
2	596.34
3	766.44
4	439.79

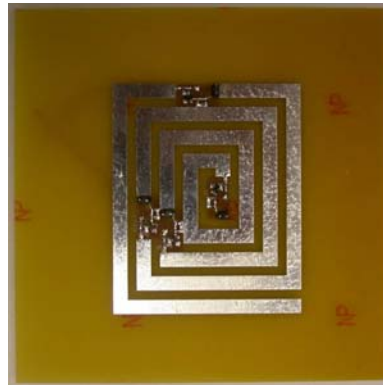
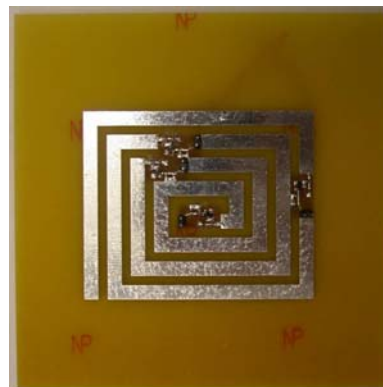


**Table A20.** Element Voltages Linear Polarization Position 4 – Uroboros

Antenna	Voltage (mV)
1	436.50
2	149.08
3	339.72
4	311.85

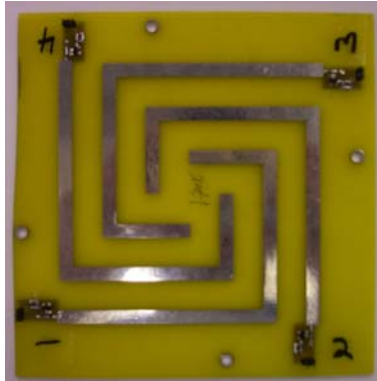


## A.2 CIRCULARLY POLARIZED

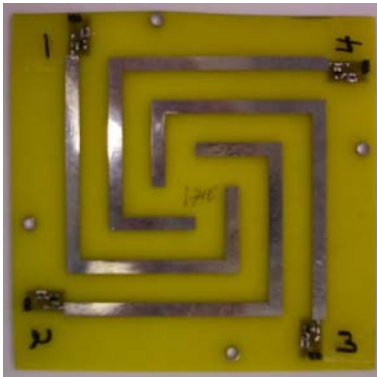
### A.2.1 Minhong

**Table A21.** Element Voltages Circular Polarization Position 1 – Minhong

		Antenna	Voltage (mV)
4	3	1	639.84
		2	606.60
1	2	3	21.51
		4	298.17



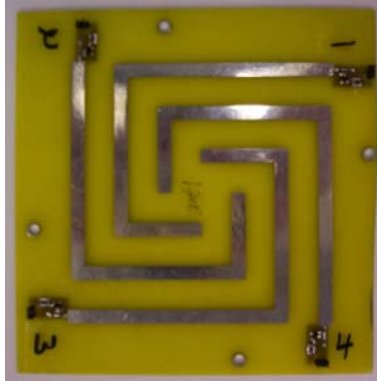
**Table A22.** Element Voltages Circular Polarization Position 2 – Minhong

		Antenna	Voltage (mV)	
1		1	349.00	
		2	618.82	
2		3	658.90	
		4	60.12	

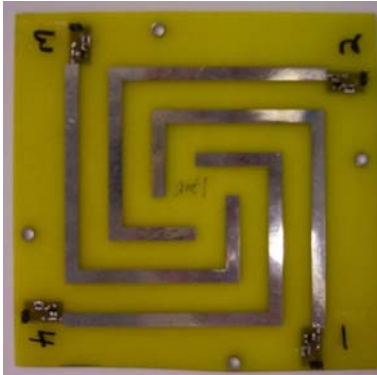
**Table A23.** Element Voltages Circular Polarization Position 3 – Minhong

2	1
3	4

Antenna	Voltage (mV)
1	164.73
2	414.01
3	553.32
4	621.75



**Table A24.** Element Voltages Circular Polarization Position 4 – Minhong

		Antenna	Voltage (mV)	
3	2	1	622.73	
		2	120.73	
4	1	3	287.90	
		4	636.91	

### A.2.2 Uncenter

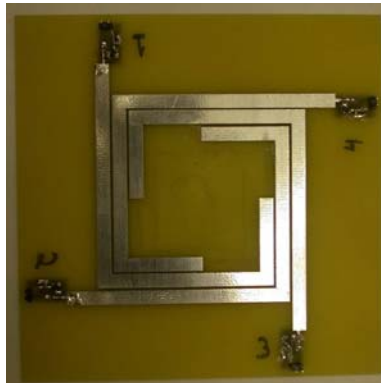
**Table A25.** Element Voltages Circular Polarization Position 1 – Uncenter

		Antenna	Voltage (mV)
4	3	1	198.45
		2	105.09
1	2	3	0.00
		4	78.70

**Table A26.** Element Voltages Circular Polarization Position 2 – Uncenter

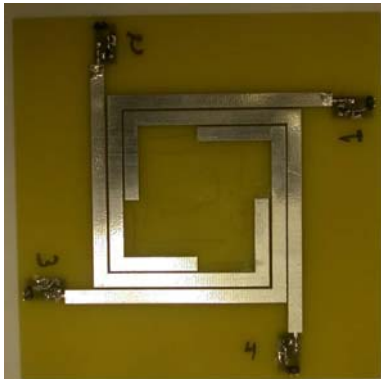
		Antenna	Voltage (mV)
1		1	109.00
		2	156.90
2		3	79.19
		4	5.38

1	4
2	3

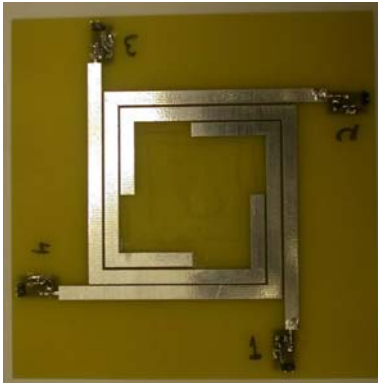


**Table A27.** Element Voltages Circular Polarization Position 3 – Uncenter

		Antenna	Voltage (mV)
2	1	1	0.00
		2	58.66
3	4	3	83.58
		4	156.42




**Table A28.** Element Voltages Circular Polarization Position 4 – Uncenter

		Antenna	Voltage (mV)	
3	2	1	140.29	
		2	4.40	
4	1	3	28.35	
		4	216.05	

### A.2.3 Sarlacc


**Table A29.** Element Voltages Circular Polarization Position 1 – Sarlacc

		Antenna	Voltage (mV)	
4	3	1	1153.57	
		2	414.50	
1	2	3	633.97	
		4	787.95	


**Table A30.** Element Voltages Circular Polarization Position 2 – Sarlacc

		Antenna	Voltage (mV)
1		1	765.48
		2	1082.69
2		3	390.55
		4	637.88

1	4
2	3



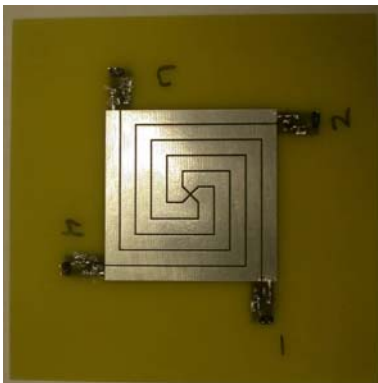
**Table A31.** Element Voltages Circular Polarization Position 3 – Sarlacc

		Antenna	Voltage (mV)	
2	1	1	643.75	
		2	781.10	
3	4	3	1114.46	
		4	400.82	

**Table A32.** Element Voltages Circular Polarization Position 4 – Sarlacc

3	2
4	1


Antenna	Voltage (mV)
1	420.37
2	651.57
3	831.44
4	1150.64



## A.2.4 Oculus

**Table A33.** Element Voltages Circular Polarization Position 1 – Oculus


		Antenna	Voltage (mV)
4	3	1	273.73
		2	362.20
1	2	3	435.52
		4	460.67



**Table A34.** Element Voltages Circular Polarization Position 2 – Oculus

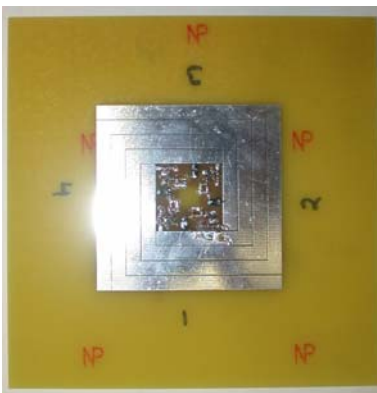
		Antenna	Voltage (mV)
1		1	409.61
		2	253.69
2	3	3	302.08
		4	479.51

**Table A35.** Element Voltages Circular Polarization Position 3 – Oculus

		Antenna	Voltage (mV)	
2	1	1	470.23	
		2	473.65	
3	4	3	246.84	
		4	368.07	

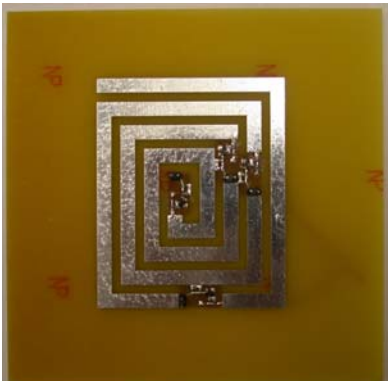


**Table A36.** Element Voltages Circular Polarization Position 4 – Oculus

<div> <div>32</div> <div>41</div> </div>	Antenna	Voltage (mV)	
	1	294.75	
	2	479.51	
	3	392.51	
	4	352.91	

## A.2.5 Uroboros

**Table A37.** Element Voltages Circular Polarization Position 1 – Uroboros

Antenna	Voltage (mV)	
1	608.56	
2	293.77	
3	132.95	
4	721.96	

**Table A38.** Element Voltages Circular Polarization Position 2 – Uroboros

Antenna	Voltage (mV)
1	563.59
2	0.00
3	311.85
4	729.29

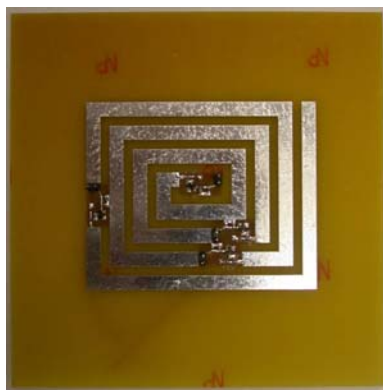


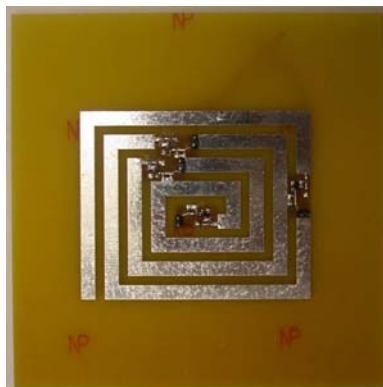
**Table A39.** Element Voltages Circular Polarization Position 3 – Uroboros

Antenna	Voltage (mV)
1	720.98
2	588.03
3	565.05
4	67.94



**Table A40.** Element Voltages Circular Polarization Position 4 – Uroboros

Antenna	Voltage (mV)
1	716.58
2	684.81
3	351.94
4	394.46



## **APPENDIX B**

### **RFID TAG EXTENDED RESULTS**

The full results of the read rate test and the maximum distance test using the TI RFID chips are presented here. The results for the Sarlacc design presented earlier are repeated for ease of comparison.

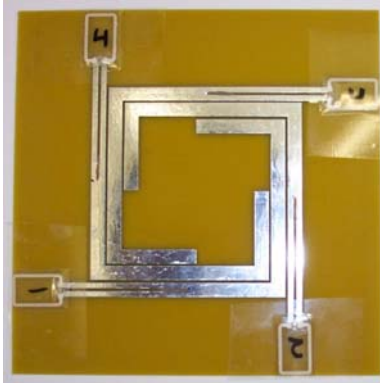
#### **B.1 READ RATES LINEAR POLARIZATION**

As stated in section 5.3.1 the Minhong design would not read at this distance and there are no results to present.

### B.1.1 Uncenter

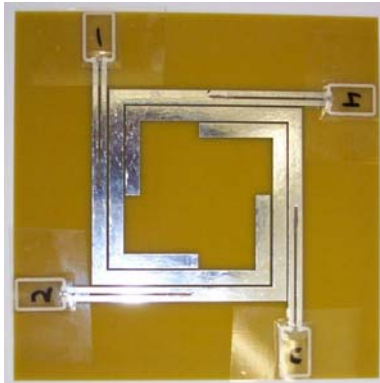
**Table B1.** Read Rate Linear Polarization Position 1 – Uncenter

	Antenna	Read Rate
4	1	-
3	2	8.6
1	3	-
2	4	8.6
	Total	17.2

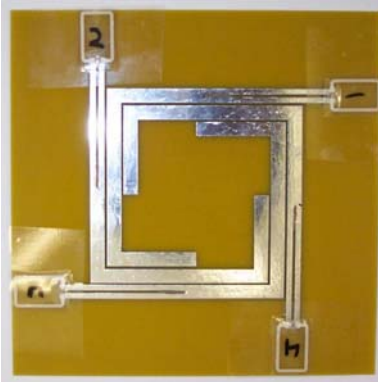


**Table B2.** Read Rate Linear Polarization Position 2 – Uncenter

		Antenna	Read Rate
1	4	1	15.6
		2	-
2	3	3	1.9
		4	-
		Total	17.5



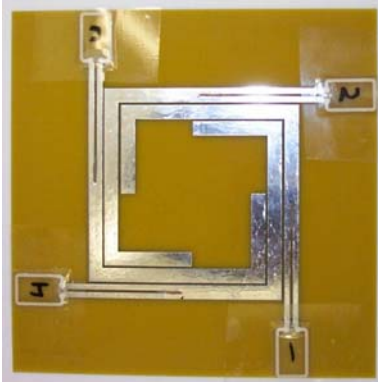
**Table B3.** Read Rate Linear Polarization Position 3 – Uncenter

		Antenna	Read Rate	
2	1	1	-	
		2	6.4	
3	4	3	6.2	
		4	5.6	
		Total	18.2	

**Table B4.** Read Rate Linear Polarization Position 4 – Uncenter

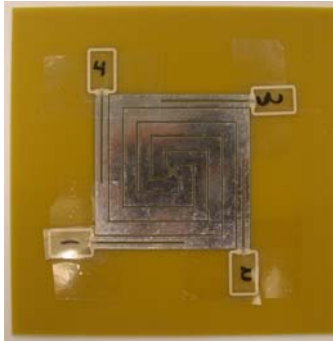
		Antenna	Read Rate
3	2	1	0.4
		2	-
4	1	3	18.1
		4	-
		Total	18.5

		Antenna	Read Rate
3	2	1	0.4
		2	-
4	1	3	18.1
		4	-
		Total	18.5



### B.1.2 Sarlacc

**Table B5.** Read Rate Linear Polarization Position 1 – Sarlacc

		Antenna	Read Rate	
4	3	1	7.2	
		2	-	
1	2	3	9.4	
		4	-	
		Total	16.6	

**Table B6.** Read Rate Linear Polarization Position 2 – Sarlacc

		Antenna	Read Rate
1	4	1	-
		2	7.4
2	3	3	-
		4	9.5
		Total	16.9

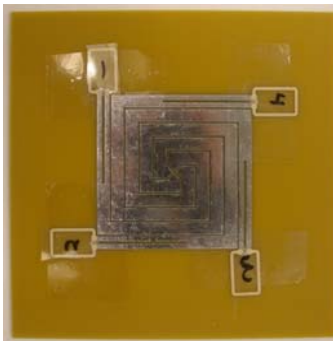


**Table B7.** Read Rate Linear Polarization Position 3 – Sarlacc

		Antenna	Read Rate
2	1	1	5.2
		2	-
3	4	3	9.2
		4	0.6
		Total	15

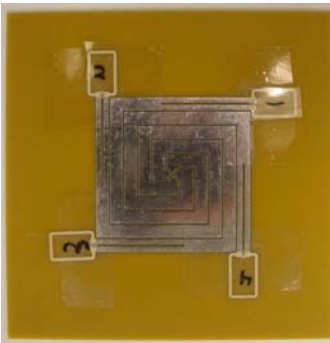
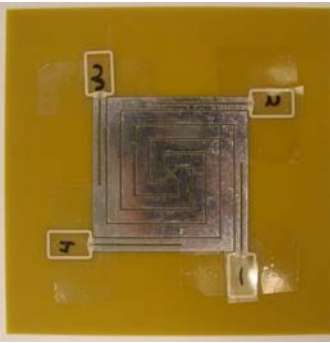


**Table B8.** Read Rate Linear Polarization Position 4 – Sarlacc

		Antenna	Read Rate
3	2	1	-
		2	6.6
4	1	3	-
		4	11.5
		Total	18.1

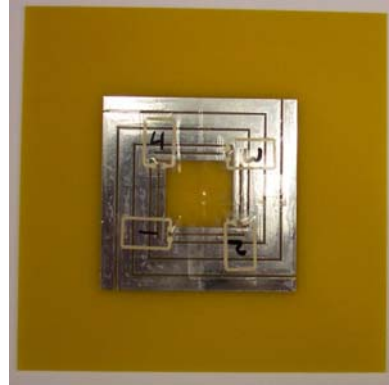
		Antenna	Read Rate
3	2	1	-
		2	6.6
4	1	3	-
		4	11.5
		Total	18.1



### B.1.3 Oculus

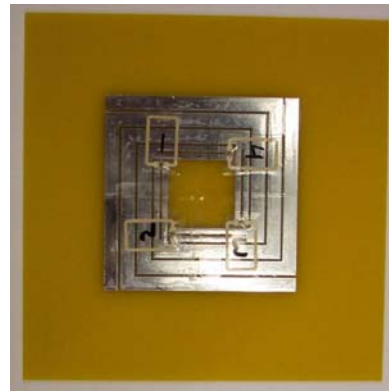
**Table B9.** Read Rate Linear Polarization Position 1 – Oculus

<div> <div>43</div> <div>12</div> </div>	Antenna	Read Rate
	1	11.7
	2	-
	3	6.6
	4	-
	Total	18.3



**Table B10.** Read Rate Linear Polarization Position 2 – Oculus

<div> <div>14</div> <div>23</div> </div>	Antenna	Read Rate
	1	-
	2	9.3
	3	-
	4	1.9
	Total	11.2



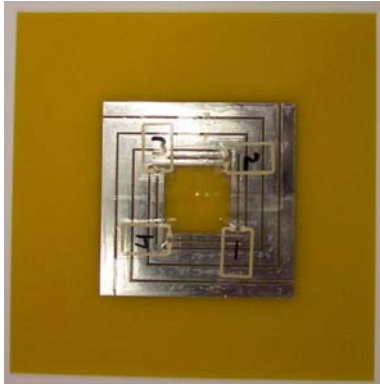


**Table B11.** Read Rate Linear Polarization Position 3 – Oculus

Antenna	Read Rate
1	10.2
2	-
3	4.2
4	-
Total	14.4

**Table B12.** Read Rate Linear Polarization Position 4 – Oculus

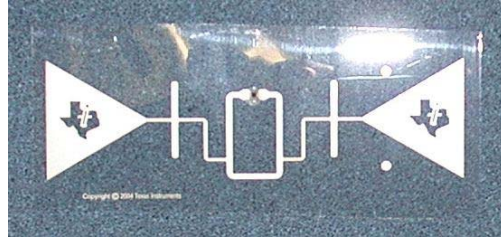
		Antenna	Read Rate
3	2	1	-
		2	5.0
4	1	3	-
		4	4.6
		Total	9.6

			
--	--	---	--

## B.1.4 TI Tag

**Table B13.** Read Rate Linear Polarization – TI Tag

Position	Read Rate
Horizontal	-
Vertical	20.0

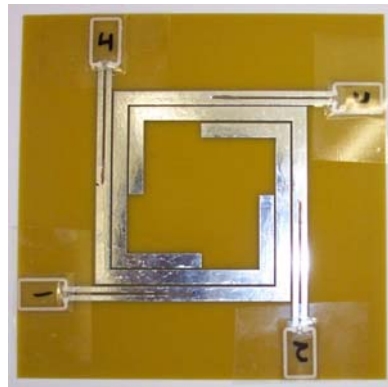


## B.2 READ RATE CIRCULAR POLARIZATION

### B.2.1 Uncenter

**Table B14.** Read Rate Circular Polarization Position 1 – Uncenter

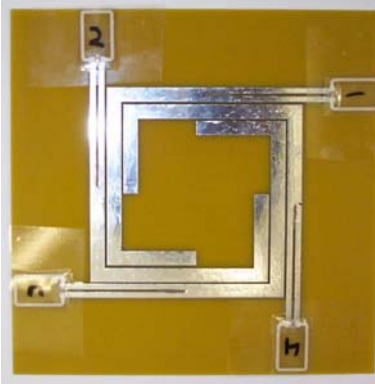
		Antenna	Read Rate
4	3	1	6.6
		2	3.0
1	2	3	1.3
		4	6.5
		Total	17.4



**Table B15.** Read Rate Circular Polarization Position 2 – Uncenter

		Antenna	Read Rate
1	4	1	4.6
		2	5.1
2	3	3	5.1
		4	3.9
		Total	18.7

**Table B16.** Read Rate Circular Polarization Position 3 – Uncenter

<table><tr><td>2</td><td>1</td></tr><tr><td>3</td><td>4</td></tr></table>		2	1	3	4	<table><tr><th>Antenna</th><th>Read Rate</th></tr><tr><td>1</td><td>8.5</td></tr><tr><td>2</td><td>7.2</td></tr><tr><td>3</td><td>-</td></tr><tr><td>4</td><td>0.6</td></tr><tr><td>Total</td><td>16.3</td></tr></table>	Antenna	Read Rate	1	8.5	2	7.2	3	-	4	0.6	Total	16.3	
2	1																		
3	4																		
Antenna	Read Rate																		
1	8.5																		
2	7.2																		
3	-																		
4	0.6																		
Total	16.3																		

**Table B17.** Read Rate Circular Polarization Position 4 – Uncenter

3	2
4	1

Antenna	Read Rate
1	3.0
2	4.2
3	4.9
4	5.5
Total	17.6

## B.2.2 Sarlace

**Table B18.** Read Rate Circular Polarization Position 1 – Sarlace

4	3
1	2

Antenna	Read Rate
1	5.0
2	4.8
3	3.0
4	4.7
Total	17.5

**Table B19.** Read Rate Circular Polarization Position 2 – Sarlacc

		Antenna	Read Rate
1	4	1	-
		2	4.5
2	3	3	1.6
		4	10.1
		Total	16.2

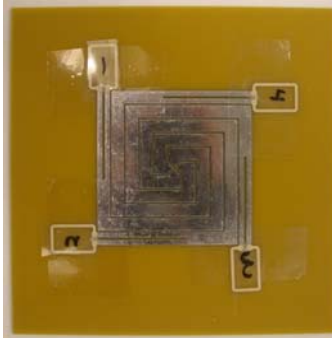


**Table B20.** Read Rate Circular Polarization Position 3 – Sarlacc

		Antenna	Read Rate
2	1	1	4.3
		2	5.6
3	4	3	3.2
		4	4.6
		Total	17.7

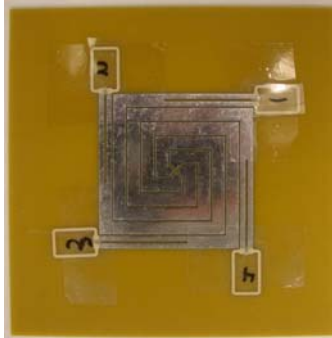
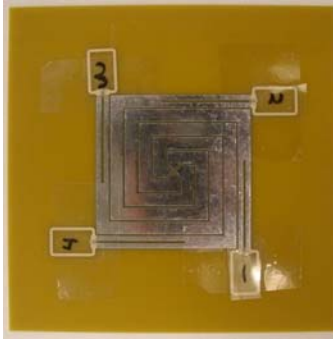


**Table B21.** Read Rate Circular Polarization Position 4 – Sarlacc


		Antenna	Read Rate
3	2	1	0.4
		2	2.6
4	1	3	5.8
		4	6.4
		Total	18.2



### B.2.3 Oculus

**Table B22.** Read Rate Circular Polarization Position 1 – Oculus

		Antenna	Read Rate
4	3	1	12.3
		2	1.6
1	2	3	1.9
		4	-
		Total	15.8



**Table B23.** Read Rate Circular Polarization Position 2 – Oculus

1	4
2	3

Antenna	Read Rate
1	8.8
2	7.0
3	1.0
4	-
Total	16.8

A photograph of a square microchip, likely a RFID tag, mounted on a larger square substrate. The chip has four small rectangular antennas labeled 1, 2, 3, and 4. The chip is mounted on a larger square substrate with a grid pattern. The background is a solid olive green color.

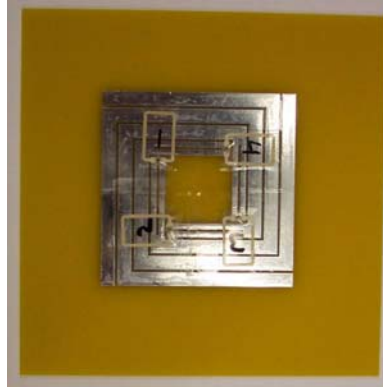


**Table B24.** Read Rate Circular Polarization Position 3 – Oculus

2	1
3	4

Antenna	Read Rate
1	9.4
2	1.7
3	4.6
4	-
Total	15.7

A photograph of a square microchip, likely a RFID tag, mounted on a blue substrate. The chip is square with a central square cutout. Four small, gold-colored rectangular pads are attached to the chip, labeled with numbers 1, 2, 3, and 4. Pad 1 is at the top, pad 2 is on the left, pad 3 is at the bottom, and pad 4 is on the right. The chip itself has a metallic, reflective surface.

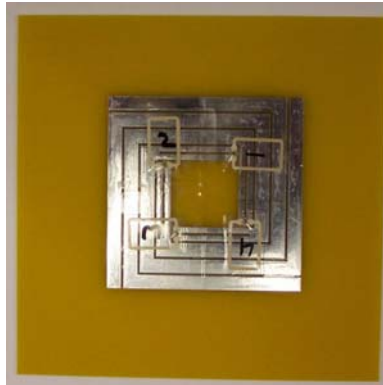
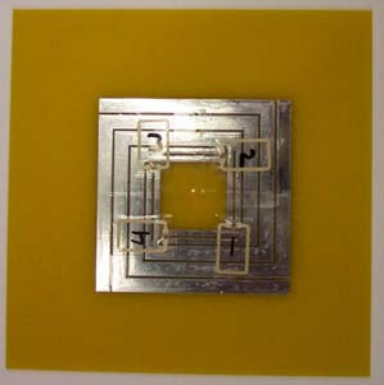


**Table B25.** Read Rate Circular Polarization Position 4 – Oculus

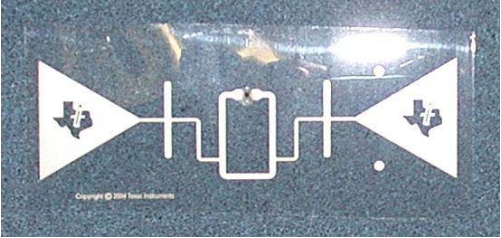
		Antenna	Read Rate
3	2	1	7.8
		2	3.3
4	1	3	4.5
		4	2.1
		Total	17.7



#### B.2.4 TI Tag

**Table B26.** Read Rate Circular Polarization– TI Tag

Position	Read Rate
Horizontal	19.2
Vertical	19.2







### B.3 READ RANGE RESULTS LINEAR POLARIZATION

#### B.3.1 Minhong – Separation: 22cm

**Table B27.** Read Range Linear Polarization Position 1 – Minhong

<div> <div>43</div> <div>12</div> </div>	Antenna	Power (dBm)	Range (m)	
	1	-	Unreadable	
	2	-	Unreadable	
	3	22	0.45	
	4	20	0.57	
	Total		1.02	

**Table B28.** Read Range Linear Polarization Position 2 – Minhong

<div> <div>14</div> <div>23</div> </div>	Antenna	Power (dBm)	Range (m)	
	1	-	Unreadable	
	2	-	Unreadable	
	3	-	Unreadable	
	4	19.5	0.57	
	Total		0.57	

**Table B29.** Read Range Linear Polarization Position 3 – Minhong

2	1
3	4

Antenna	Power (dBm)	Range (m)
1	-	Unreadable
2	27	0.25
3	-	Unreadable
4	22	0.45
Total		0.7



**Table B30.** Read Range Linear Polarization Position 4 – Minhong

3	2
4	1

Antenna	Power (dBm)	Range (m)
1	-	Unreadable
2	-	Unreadable
3	27	0.25
4	-	Unreadable
Total		0.25

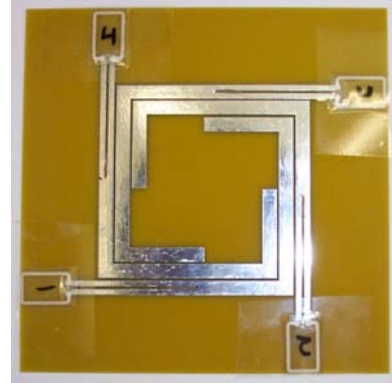


### B.3.2 Uncenter – Separation: 60cm

**Table B31.** Read Range Linear Polarization Position 1 – Uncenter

4	3
1	2

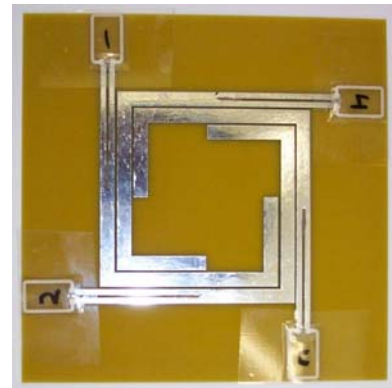
Antenna	Power (dBm)	Range (m)
1	-	Unreadable
2	21.5	1.23
3	-	Unreadable
4	26	0.78
Total		2.01



**Table B32.** Read Range Linear Polarization Position 2 – Uncenter

1	4
2	3

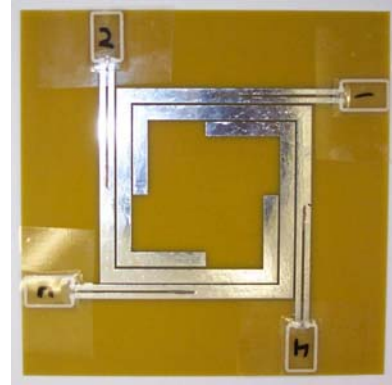
Antenna	Power (dBm)	Range (m)
1	23	1.10
2	-	Unreadable
3	21	1.38
4	-	Unreadable
Total		2.48



**Table B33.** Read Range Linear Polarization Position 3 – Uncenter

2	1
3	4

Antenna	Power (dBm)	Range (m)
1	-	Unreadable
2	25.5	0.78
3	-	Unreadable
4	23.5	0.98
Total		1.76

**Table B34.** Read Range Linear Polarization Position 4 – Uncenter

3	2
4	1

Antenna	Power (dBm)	Range (m)
1	20	1.55
2	-	Unreadable
3	23.5	0.98
4	-	Unreadable
Total		2.53



### B.3.3 Sarlacc – Separation: 70cm

**Table B35.** Read Range Linear Polarization Position 1 – Sarlacc

<div> <div>43</div> <div>12</div> </div>	Antenna	Power (dBm)	Range (m)	
	1	19.5	1.81	
	2	-	Unreadable	
	3	20.5	1.81	
	4	-	Unreadable	
	Total		3.62	

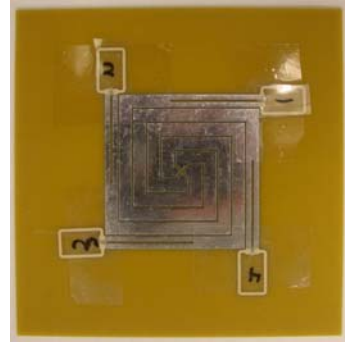
**Table B36.** Read Range Linear Polarization Position 2 – Sarlacc

<div> <div>14</div> <div>23</div> </div>	Antenna	Power (dBm)	Range (m)	
	1	-	Unreadable	
	2	20.5	1.81	
	3	-	Unreadable	
	4	17.5	2.28	
	Total		4.09	

**Table B37.** Read Range Linear Polarization Position 3 – Sarlacc

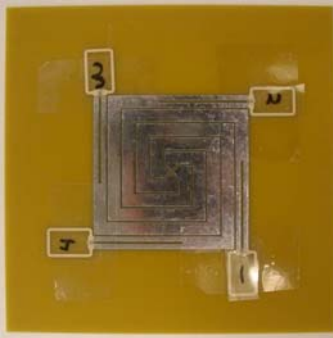
2	1
3	4

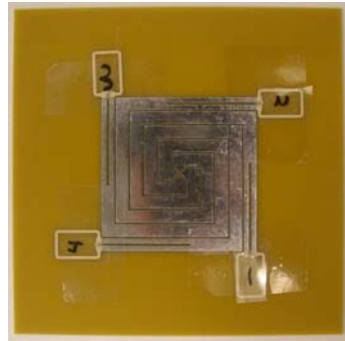
Antenna	Power (dBm)	Range (m)
1	20.5	1.81
2	-	Unreadable
3	19.5	1.81
4	-	Unreadable
Total		3.62



**Table B38.** Read Range Linear Polarization Position 4 – Sarlacc

		Antenna	Power (dBm)	Range (m)
3	2	1	-	Unreadable
		2	22	1.44
4	1	3	-	Unreadable
		4	17	2.55
		Total		3.99



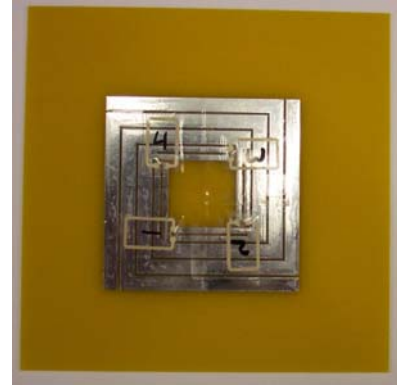


### B.3.4 Oculus – Separation: 50cm

**Table B39.** Read Range Linear Polarization Position 1 – Oculus

4	3
1	2

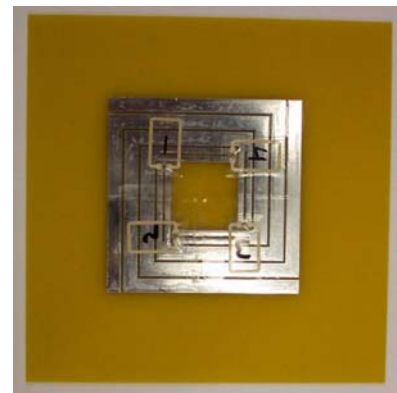
Antenna	Power (dBm)	Range (m)
1	22.5	1.03
2	-	Unreadable
3	-	Unreadable
4	-	Unreadable
Total		1.03



**Table B40.** Read Range Linear Polarization Position 2 – Oculus

1	4
2	3

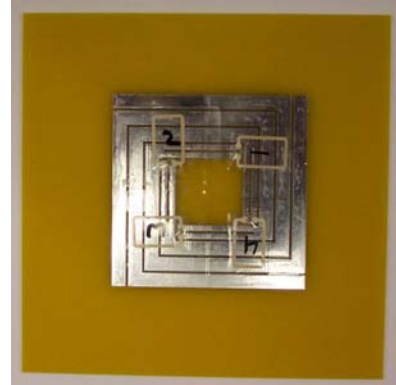
Antenna	Power (dBm)	Range (m)
1	-	Unreadable
2	23.5	0.81
3	-	Unreadable
4	-	Unreadable
Total		0.81



**Table B41.** Read Range Linear Polarization Position 3 – Oculus

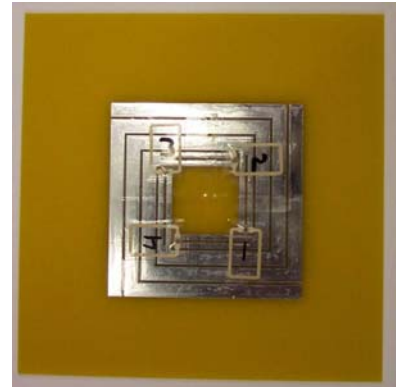
2	1
3	4

Antenna	Power (dBm)	Range (m)
1	23.5	0.81
2	-	Unreadable
3	26	0.65
4	-	Unreadable
Total		1.46

**Table B42.** Read Range Linear Polarization Position 4 – Oculus

3	2
4	1

Antenna	Power (dBm)	Range (m)
1	-	Unreadable
2	25	0.73
3	-	Unreadable
4	25.5	0.65
Total		1.38

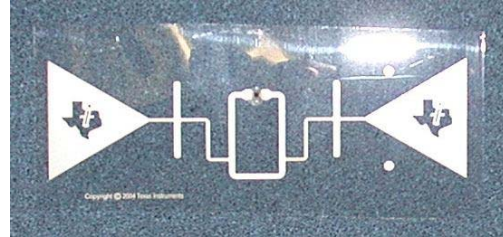




### B.3.5 TI Tag – Separation 70cm

**Table B43.** Read Range Linear Polarization– TI Tag

Position	Power (dBm)	Range (m)
Vertical	15.5	2.86
Horizontal	-	Unreadable



## B.4 READ RANGE RESULTS CIRCULAR POLARIZATION

### B.4.1 Minhong – Separation: 35cm

**Table B44.** Read Range Circular Polarization Position 1 – Minhong

Antenna	Power (dBm)	Range (m)
1	-	Unreadable
2	-	Unreadable
3	29.5	0.39
4	22.5	0.98
Total		1.37

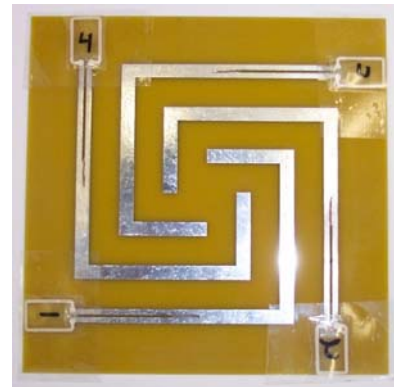


**Table B45.** Read Range Circular Polarization Position 2 – Minhong

1	4	Antenna	Power (dBm)	Range (m)
		1	-	Unreadable
2	3	2	-	Unreadable
		3	-	Unreadable
		4	24	0.78
Total				0.78



**Table B46.** Read Range Circular Polarization Position 3 – Minhong


2	1	Antenna	Power (dBm)	Range (m)
		1	-	Unreadable
3	4	2	-	Unreadable
		3	31	0.35
		4	25	0.71
Total				1.06



**Table B47.** Read Range Circular Polarization Position 4 – Minhong

3	2
4	1

Antenna	Power (dBm)	Range (m)
1	-	Unreadable
2	-	Unreadable
3	27.5	0.49
4	24.5	0.78
Total		1.27



#### B.4.2 Uncenter – Separation: 70cm

**Table B48.** Read Range Circular Polarization Position 1 – Uncenter

4	3
1	2

Antenna	Power (dBm)	Range (m)
1	21.5	1.97
2	24.5	1.56
3	23.5	1.56
4	28	0.99
Total		6.08

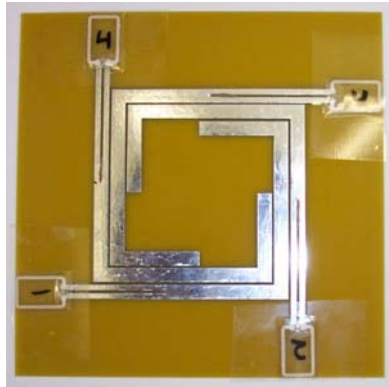


**Table B49.** Read Range Circular Polarization Position 2 – Uncenter

1	4
2	3

Antenna	Power (dBm)	Range (m)
1	25.5	1.24
2	23.5	1.56
3	23	1.75
4	26	1.24
Total		5.79

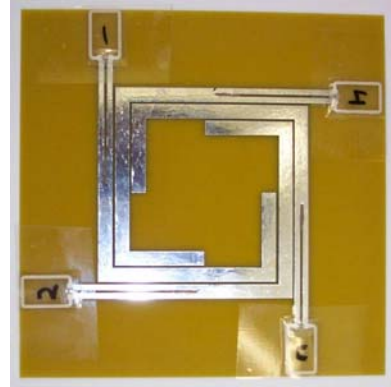


**Table B50.** Read Range Circular Polarization Position 3 – Uncenter

Antenna	Power (dBm)	Range (m)
1	22	1.97
2	26.5	1.24
3	22.5	1.97
4	26.5	1.24
Total		6.42

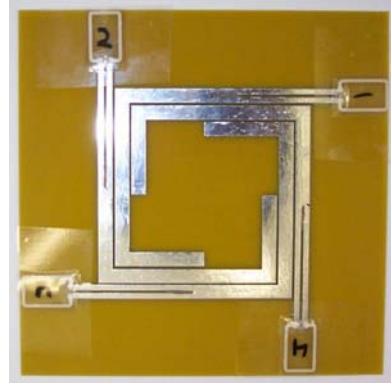
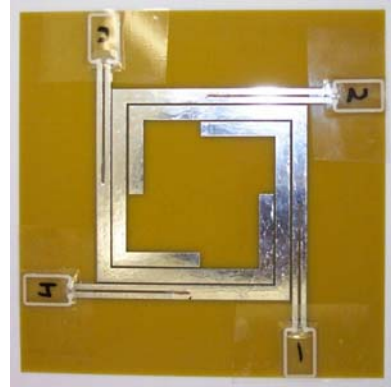


**Table B51.** Read Range Circular Polarization Position 4 – Uncenter

3	2
4	1

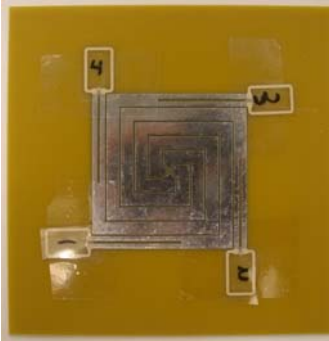
Antenna	Power (dBm)	Range (m)
1	23.5	1.56
2	24.5	1.56
3	24.5	1.56
4	24.5	1.56
Total		6.24



#### B.4.3 Sarlacc – Separation: 70cm

**Table B52.** Read Range Circular Polarization Position 1 – Sarlacc

		Antenna	Power (dBm)	Range (m)
4	3	1	20.5	2.47
		2	19.5	2.47
1	2	3	22.5	1.97
		4	16.5	3.92
		Total		10.83



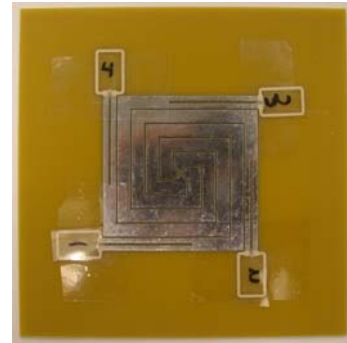


**Table B53.** Read Range Circular Polarization Position 2 – Sarlace

1	4
2	3

Antenna	Power (dBm)	Range (m)
1	18.5	3.12
2	22.5	1.97
3	18.5	3.12
4	19.5	2.47
Total		10.68

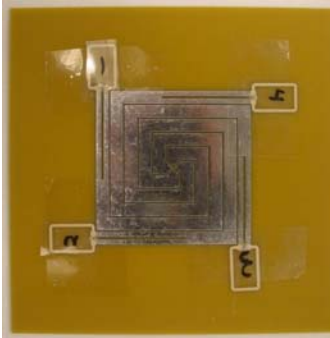


**Table B54.** Read Range Circular Polarization Position 3 – Sarlace

2	1
3	4

Antenna	Power (dBm)	Range (m)
1	21	2.21
2	20	2.47
3	21.5	1.97
4	15.5	3.92
Total		10.57

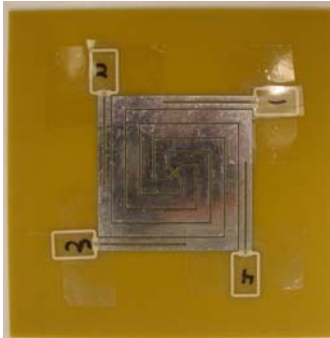
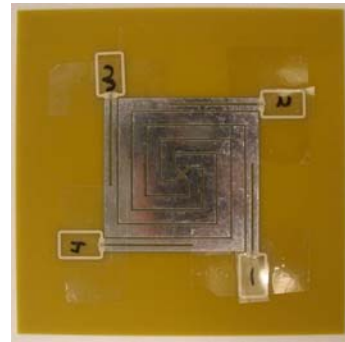


**Table B55.** Read Range Circular Polarization Position 4 – Sarlacc

3	2
4	1

Antenna	Power (dBm)	Range (m)
1	18.5	3.12
2	23.5	1.56
3	18.5	3.12
4	18.5	3.12
Total		10.92



#### B.4.4 Oculus – Separation: 70cm

**Table B56.** Read Range Circular Polarization Position 1 – Oculus

4	3
1	2

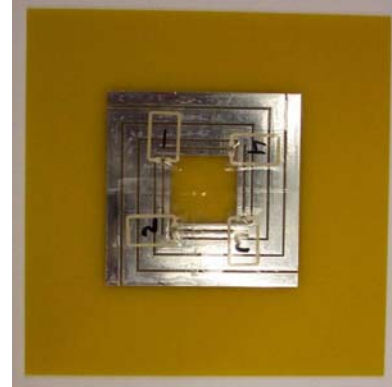
Antenna	Power (dBm)	Range (m)
1	29	0.88
2	28	0.99
3	-	Unreadable
4	30	0.78
Total		2.65



**Table B57.** Read Range Circular Polarization Position 2 – Oculus

1	4
2	3

Antenna	Power (dBm)	Range (m)
1	26.5	1.24
2	30.5	0.78
3	29.5	0.78
4	-	Unreadable
Total		2.8

**Table B58.** Read Range Circular Polarization Position 3 – Oculus

2	1
3	4

Antenna	Power (dBm)	Range (m)
1	30.5	0.78
2	28	0.99
3	-	Unreadable
4	30	0.78
Total		2.55

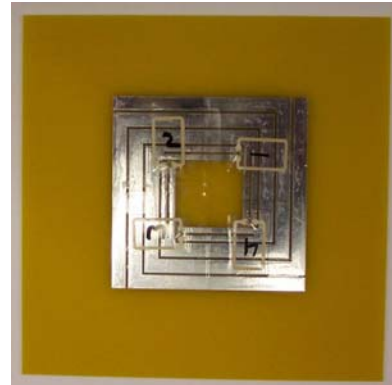
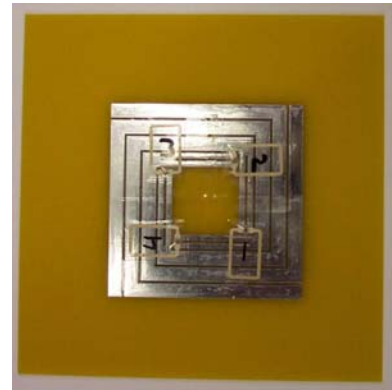




**Table B59.** Read Range Circular Polarization Position 4 – Oculus

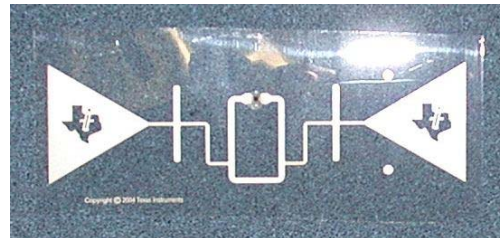
Antenna	Power (dBm)	Range (m)
1	26.5	1.24
2	-	Unreadable
3	30	0.78
4	-	Unreadable
Total		2.02



#### B.4.5 TI Tag – Separation 70cm

**Table B60.** Read Range Circular Polarization– TI Tag

Position	Power (dBm)	Range (m)
Vertical	16.5	3.92
Horizontal	14	4.94



## BIBLIOGRAPHY

- [1] Marlin H. Mickle , Minhong Mi, Chris Capelli, and Harold Swift, "RF Energy Harvesting with Multiple Antennas in the Same Space", IEEE Antennas and Propagation Magazine, Vol. 47, No. 5, Dec. 2005, pp. 100-106.
- [2] Marlin H. Mickle, Minhong Mi, Leonid Mats, Chris Capelli, and Harold Swift, "Powering Autonomous Cubic-Millimeter Devices", IEEE Antennas and Propagation Magazine, Vol. 48, No. 1, Feb. 2006, pp. 11-21.
- [3] Carlos E. Saavedra and Brad R. Jackson, "Voltage-Variable Attenuator MMIC using Phase Cancellation," IEEE Proceedings Circuits, Devices, and Systems, May 2006.
- [4] Jean-Fu Kiang, Novel Technologies for Microwave and Millimeter-Wave Applications, Kluwer, Boston, 2004, p.226.
- [5] Impinj, "The RFID Antenna: Maximum Power Transfer", Rev 1.0, Oct 2005, <http://www.impinj.com>
- [6] "Antenna Reflectors," Air Force Manual, No. 52-19, 1953, pp.144-145.
- [7] Charles Edward Greene, "On-Chip Impedance Transformations for a Standard CMOS Process," Thesis University of Pittsburgh, 2002
- [8] K. V. Seshagiri Rao, Pavel V. Nikitin, Sander F. Lam, "Antenna Designs for UHF RFID Tags: A Review and a Practical Application", IEEE Transactions on Antennas and Propagation, Vol. 53, No. 12, Dec. 2005, pp.3870-3876.
- [9] U.S. Federal Communications Commission, Office of Engineering and Technology, "Evaluating Compliance with FCC Guidelines for Human Exposure to Radiofrequency Electromagnetic Fields", OET Bulletin 65, Edition 97-01, pp.3, 27-30, August 1997.
- [10] EPC Global, "EPC™ Radio-Frequency Identity Protocols Class-1 Generation-2 UHF RFID," Version 1.0.9, Jan 2005, <http://www.epcglobalinc.org>